ADVANCED MATERIALS
www.advmat.de

www.MaterialsViews.com

Size Effects on Magnetic Actuation in Ni-Mn-Ga Shape-Memory Alloys

David C. Dunand and Peter Müllner*

The off-stoichiometric Ni_2MnGa Heusler alloy is a magnetic shape-memory alloy capable of reversible magnetic-field-induced strains (MFIS). These are generated by twin boundaries moving under the influence of an internal stress produced by a magnetic field through the magnetocrystalline anisotropy. While MFIS are very large (up to 10%) for monocrystalline Ni-Mn-Ga, they are near zero (<0.01%) in fine-grained polycrystals due to incompatibilities during twinning of neighboring grains and the resulting internal geometrical constraints. By growing the grains and/or shrinking the sample, the grain size becomes comparable to one or more characteristic sample sizes (film thickness, wire or strut diameter, ribbon width, particle diameter, etc), and the grains become surrounded by free space. This reduces the incompatibilities between neighboring grains and can favor twinning and thus increase the MFIS. This approach was validated recently with very large MFIS (0.2–8%) measured in Ni-Mn-Ga fibers and foams with bamboo grains with dimensions similar to the fiber or strut diameters and in thin plates where grain diameters are comparable to plate thickness. Here, we review processing, micro- and macrostructure, and magneto-mechanical properties of (i) Ni-Mn-Ga powders, fibers, ribbons and films with one or more small dimension, which are amenable to the growth of bamboo grains leading to large MFIS, and (ii) "constructs" from these structural elements (e.g., mats, laminates, textiles, foams and composites). Various strategies are proposed to accentuate this geometric effect which enables large MFIS in polycrystalline Ni-Mn-Ga by matching grain and sample sizes.

1. Introduction

1.1. Motivation

Magnetic shape-memory alloys (MSMAs) are multi-functional materials exhibiting coupling between magnetic and structural order which leads to a very large magnetic-field-induced strain (MFIS). This effect, which is also referred to as the "magnetic shape-memory effect", arises through the magnetic-field-induced motion of twin boundaries.[1,2] Because the MFIS may be permanent or reversible upon removal of the magnetic field, the terms "magnetoplasticity" and "magnetoelasticity" are also used.[3] While the magnetic shape-memory effect is useful for actuation purposes, the inverse effect may be utilized for sensing and energy harvesting applications.[4] In combination, the direct and inverse magnetic shape-memory effects cause magnetic-field-induced superelasticity, which is the magnetically-induced recovery of a large mechanically-induced deformation.[5] Magnetic-field-induced superelasticity can also be utilized for energy harvesting.[6,7]

MSMAs are also shape-memory alloys in the traditional sense,[1,2] i.e., they exhibit a thermoelastic martensite transformation and may change their shape between two states continuously upon heating and cooling.[8] The martensitic transformation may be stress-induced, which causes superelasticity. The coupling between magnetic and structural ordering in conjunction with the magnetic and structural transformations give rise to further functional (i.e., non mechanical) properties: the magnetocaloric effect,[9] the magnetic-field-induced martensitic transformation and its reverse transformation,[10] and giant magnetoresistance.[11]

So far, large MFIS values (~1–10%) have been reported for Ni-Mn-Ga single crystals as reviewed in refs. [12–15]. Polycrystalline Ni-Mn-Ga with small grains shows vanishingly small MFIS (<0.01%) because grain boundaries are very effectively suppressing the motion of twin boundaries, or equivalently, neighboring grains have incompatible MFIS. Larger MFIS of ~0.1–1% can be generated in magnetically trained, highly textured, coarse-grained samples.[16] These so-called oligocrystals (defined as materials with low numbers of grains relative to their volume[17,18]) are intermediate between mono- and polycrystals. Recently, large MFIS (2–9%) were also demonstrated in polycrystalline samples in which high level of porosity were introduced, which reduce incompatibilities between grains,[19] as discussed in detail in Section 1.2.

It is of both technological and fundamental interest to overcome the hindrance of grain boundaries (and other constraints)

Prof. D. C. Dunand
Department of Materials Science & Engineering
Northwestern University
Evanston, Illinois 60208, USA
E-mail: dunand@northwestern.edu
Prof. P. Müllner
Department of Materials Science & Engineering
Boise State University
Boise, Idaho 83725, USA

DOI: 10.1002/adma.201002753

which suppress magnetic-field-induced actuation of MSMAs. The fabrication of single crystals is time-consuming and difficult, and chemical segregation during the growth process reduces the performance of the crystals. Also, the operation frequency of MSMA transducers is limited by eddy currents and inertia[20] which both decrease with decreasing sample size. Thus, further technological opportunities arise when miniaturizing MSMA-based devices based on small-size MSMA particles, fibers, ribbons, films, bi- and multilayers, pillars, etc.

The present Progress Report aims to review the state of the art on MSMAs at small length scales, with emphasis on MFIS. "Small" here does not necessarily refer to an absolute value. As discussed by Arzt,[21] size effects arise when a "characteristic length" (which is related to the mechanics of a phenomenon) interacts with a size parameter (e.g., grain size, film thickness, fiber diameter). Strategies for increasing MFIS in mono-, oligo-, and polycrystalline Ni-Mn-Ga structures at small size are also being discussed. This includes preparation and processing which are key to achieving grain sizes similar to sample size. While other MSMAs exist and are being further developed,[1,2,22] large MFIS at room temperature was demonstrated so far only for Ni-Mn-Ga, which is the alloy on which the present report focuses.

1.2. Background

The magnetic-field-induced motion of twin boundaries results from a strong coupling of magnetic and structural order. This coupling generates an interaction between magnetic and crystallographic domains (i.e., crystallographic twins) and is expressed by the magnetocrystalline anisotropy constant K_u. At small magnetic field strength, the mechanical stress is proportional to the magnetic field which produces it. At a magnetic field strength larger than the saturation field (which is proportional to K_u), the magnetic domains decouple from the crystallographic domains. The upper limit of the maximum normal stress σ_{max} due to a magnetic field is, thus, controlled by the anisotropy constant [1,23]:

$$\sigma_{max} = \frac{K_u}{\varepsilon_{max}}. \quad (1)$$

were ε_{max} is the maximum strain attainable by twinning given by the lattice parameters, as discussed below.

On a microscopic scale, twin boundary motion occurs by the motion of twinning disconnections, which are line defects at interfaces with a Burgers vector (similar to dislocations) and an additional step component.[24–26] In many situations, a set of twinning disconnections of a given twin boundary behaves similarly to a dislocation pile-up.[27–29] In some situations, e.g., for twin-twin interaction[30] and in hierarchically twinned martensite,[3] the step character of the disconnections plays a critical role. In these situations, twinning disconnections form disconnection walls and can be considered as arrays of disclinations.[3,31]

Twinning disconnections are susceptible to various fields.[30] A stress field interacts with the strain field of the disconnection, which is given by the dislocation character, i.e. by the Burgers vector. Thus, the response of a twinning disconnection to a stress field is governed by the Peach-Koehler equation, which describes the mechanical force exerted by a stress field on a dislocation. For a ferromagnetic material, a magnetic field generates a magnetic force on the disconnection, which is proportional to the step component. The magnetic force is limited by the magnetocrystalline anisotropy constant. A balance of the magnetic and mechanical forces yields the maximum magneto-stress $\tau_{M,max}$, which is a shear stress given by:[32]

$$\tau_{M,max} = \frac{K_u}{s_t} \quad (2)$$

where s_t the twinning shear strain, which equals the ratio of the Burgers vector and the step height. The maximum normal stress, which can be supported by a magnetic field (also referred to as the 'blocking stress'[33]), is twice the magneto-stress. **Table 1** provides an overview for MSMAs for which MFIS was demonstrated. Listed are values for K_u, s_t, $2\tau_{M,max}$, the experimental twinning stress σ_t, and the experimental MFIS. Significant MFIS is expected if the magneto-stress is larger than half the twinning stress:[34]

Prof. David Dunand earned a Materials Science diploma (BS/MS) at the Swiss Federal Institute of Technology (ETH Zürich) in 1986 and a Materials Science and Engineering Ph.D. at the Massachusetts Institute of Technology in 1991. As the James and Margie Krebs Professor of Materials Science and Engineering at Northwestern University, his research focuses on physical metallurgy of bulk, composite, and porous alloys. He is also co-director of the Initiative for Sustainability and Energy at Northwestern.

Prof. Peter Müllner received his diploma and doctoral degrees in Materials Science and Engineering from the ETH Zürich in 1991 and 1994. After post-doctoral studies at the University of Illinois at Urbana-Champaign, at the Max-Planck-Institute of Metals in Stuttgart, Germany, and in the Physics Department at ETH Zürich, he joined the Materials Science and Engineering Department at Boise State University in 2004. His research focuses on deformation mechanisms and on magnetic shape-memory alloys.

Table 1. Properties of ferromagnetic alloys which deform by twinning and demonstrate MFIS[1].

Material	magnetic anisotropy energy K_u (MJ/m^3)	twinning shear strain* s_t (-)	magneto-stress ** $2\tau_{M,max}$ (MPa)	Twinning stress σ_t (MPa)	saturation magnetic field $\mu_0 H_a$ (T)	MFIS (%)
Ni-Mn-Ga (10 M)	0.3–0.43 [34] 0.145 [41] 0.15–0.3 [42]	0.12	5–7	0.05–2 [38]	1 [34] 1–7 [42]	6 [196]
Ni-Mn-Ga (14 M)	0.18–0.3 [34] 0.16 [40]	0.2	2–3	1 [34]	1 [34]	10 [41]
Ni-Mn-Ga (2 M)	0.2–0.6 [34] –0.2. –0.6 [39] [43]	0.4	1–3	~10 [34]	~2 [34]	0.12 [197]
Fe-Pd	–0.05 – –0.2 [198]	0.05–0.12	2–3	1–2 [198]	0.7 [198]	0.6 [37]
Fe_3Pt	–	0.02–0.11	–	–	–	0.9 [199]
Dy	44 [36]	0.35	250	–	30 [36]	3.8 [36]

[1]CoPt is not in table, as MIR was demonstrated [199] but no MFIS data are available. *calculated from Equation (5), using published lattice parameters **calculated from Equation (2).

$$\tau_{M,\max} > \sigma_t/2 \tag{3}$$

There are many ferromagnetic materials that deform by twinning. However, only a small number meets Equation (3). Dysprosium with a MFIS of up to 3.8% MFIS,[35,36] has a very low Curie temperature (85 K) and requires an enormous field for magnetic-field-induced twin boundary motion. For $Fe_{70}Pd_{30}$, an MFIS of 0.6% was found below room temperature.[37] Ni-Mn-Ga is unique, as it exhibits a large MFIS of up to 10% at room temperature at moderate magnetic field strength due to a combination of relatively strong magnetic anisotropy and very low twinning stress (<0.1 MPa[38]). The values for the magnetic anisotropy constant varies between 0.14 and 0.6 MJ/m^3, depending on composition, martensite structure and temperature (see e.g., refs. [39–43] and references therein). The temperature dependence of K_u is given for particular compositions in refs. [34,42,43]. As a rule, K_u increases with decreasing temperature. The low twinning stress results from a phonon instability[44] and a small Burgers vector[45] and also depends on temperature (see e.g. ref. [42]).

Different descriptions of the martensite structure of Ni-Mn-Ga are found in the literature where each approach emphasizes certain properties. For example, a complete crystallographic description of the modulated martensite requires a large unit cell covering the modulation period.[46] This description is most useful for indexing diffraction patterns. For discussing magneto-mechanics, it is more convenient to refer to a pseudo-tetragonal lattice (for 10 M martensite) and a pseudo-orthorhombic lattice (for 14 M martensite). In these descriptions, the unit cell derives from a distortion of the cubic unit cell. The lattice modulation is neglected in this approach. Here, the maximum MFIS ε_{max} and the twinning shear strain s_t of the (101) $[10\bar{1}]$ twinning system are given by the lattice parameters a and c as

$$\varepsilon_{\max} = 1 - \frac{c}{a} \tag{4}$$

and

$$s_t = \frac{a}{c} - \frac{c}{a} \tag{5}$$

Since this review focuses on magneto-mechanical properties, we refer to the pseudo-tetragonal and pseudo-orthorhombic axis system,[41] e.g., when discussing the texture of films.

As summarized above, twinning proceeds via the motion of twinning disconnections. Since disconnections react to a stress field via their Burgers vector, dislocation theory applies for disconnection-disconnection interactions. This is also the case for disconnection-interface interaction.[30] Therefore, the effect of the grain structure in a polycrystalline aggregate can be understood very analogously to the grain-size hardening of alloys. Twinning disconnections form pile-ups at grain boundaries causing a back-stress on the disconnection source and finally leading to the classical Hall-Petch hardening. The resulting twinning stress is then above the magneto-stress so that MFIS is suppressed. The pile-ups further lead to stress concentrations. Under mechanical loading, the brittleness of grain boundaries in Ni-Mn-Ga causes relaxation by fracture.

1.3. Small Structures

Mechanical properties of materials with reduced size have been studied by various methods, e.g., nanoindentation,[47,48] tension-torsion testing of wires,[49] bending of thin foils[50] and beams,[51] microtensile testing,[52] and compression tests of pillars.[53–55] In all cases, the yield strength was found to increase with decreasing size. A large change of mechanical properties is expected when the size of an object is comparable to the characteristic length relevant for the primary deformation mechanism.[21] For dislocation-mediated processes, the characteristic length is of order 1 μm. Since twinning is a disconnection-mediated process, which resembles in many ways dislocation-mediated processes, it is reasonable to assume that the characteristic length is of a similar order.

For polycrystalline small-scale objects, the grain size and the sample size may both interact with the characteristic length of the deformation mechanism. As the grain size of Ni-Mn-Ga becomes comparable to one or more characteristic sample sizes (e.g., film thickness, wire or strut diameter, ribbon width, particle radius), the grains become increasingly surrounded by free space rather neighboring grains, thus decreasing the mismatch associated with twinning. An alternate description is that grain boundaries which are obstacle to the motion of twinning disconnections are replaced by free surfaces, which are not obstacles to their motion. Thus, reduced sizes in one or more dimensions may enable

MFIS in polycrystalline Ni-Mn-Ga. Reduced size also impacts magnetic interaction. Ganor et al.[56] demonstrated an increase of the blocking stress by more than a factor two and an even larger increase of the work output by reducing the sample diameter to 200 μm. This improvement results from an enhancement of the energy barrier to the rotation of the magnetization, i.e., an increase of the anisotropy energy with decreasing sample size.

A range of constructs can be conceived in which these principles are expressed in different ways and to different extent. **Figure 1** illustrates the various one-, two- and three- dimensional "structural elements" (1D: fibers and ribbon; 2D: films; 3D: powders), in which bamboo grains, spanning at least one dimension of the "structural element", can be created. While all the above shapes are three-dimensional, we use the above 1D and 2D shorthand to stress that one or two dimensions are much larger than the other(s). Also shown in Figure 1 are three-dimensional (3D) "constructs" (mats, laminates, textiles, foams and composites) which can be assembled from the above structural elements with bamboo grains. Each of these elements and constructs are reviewed in the following sections with particular focus on their processing and grain structure, and the resulting MFIS.

2. Structural Elements with One or More Small Dimensions

Structural elements may be classified according to the number of dimensions along which they are small: three for particles and powders, two for fibers, and one for films or foils. Pillars and ribbons may be considered borderline cases between particle and fiber and between fibers and foils, respectively.

2.1. Powders

Various methods have been developed to produce powders from Ni-Mn-Ga (and related MSMA[57,58]):

(i) *Spark erosion of bulk Ni-Mn-Ga*, where liquid droplets are rapidly solidified in liquid nitrogen or argon[59–61] (**Figure 2**). This method, which creates a mixture of mono- and polycrystalline powders after annealing,[62] has the disadvantage of low production volumes and potential losses of Mn and Ga during melting. Much higher production volumes could be achieved by the method of melt spraying, which however produces powders with a fine-grain structure due to the rapid solidification.

(ii) *Crushing of bulk, coarse-grained Ni-Mn-Ga* produces submillimeter powders,[63] which can further be ball-milled to achieve micron- or even sub-micrometer sizes[64–67] (**Figure 3**). For crushed powders, the brittle nature of the grain boundaries facilitates the creation of monocrystalline powders, but powder size distribution can be broad (thus limiting yield) and powder sizes are coarse (rarely below 100 μm). Ball milling provides much finer powders, but creates a disordered crystal structure with suppression of the Curie transition and austenite-martensite transformations.[64–67] The Heusler structure is however recovered upon annealing, but the powders probably remain polycrystalline.[64–67]

(iii) *Mechanical alloying* from elemental Ni, Mn and Ga powders, during which repeated breaking and welding of the powders leads to ambient-temperature synthesis of a homogenous alloy. This method has the advantage of eliminating casting (or melting) of a Ni-Mn-Ga alloy ingot as the first step of creating powders. This method is however associated with handling toxic Ni powders, and some losses of Ga which necessitate adjustments of initial powder amounts.[68] Contamination due to oxides present on the elemental powders (in particular Mn) or from wall and ball materials may also be an issue. Finally, the powders have a highly disordered structure necessitating an annealing step to achieve the Heusler phase.[68]

(iv) *Crushing or milling of Ni-Mn-Ga fibers* which were annealed to achieve a bamboo grain structure, with grain sizes similar to fiber cross-section (**Figure 4**). Two of the three dimensions of the powders are given by the diameter of the fibers which are likely to fracture at grain boundaries, yielding monocrystalline powders with narrower size distribution, as reported in refs. [69,70]. Production volumes are however limited by the creation of Ni-Mn-Ga fibers.

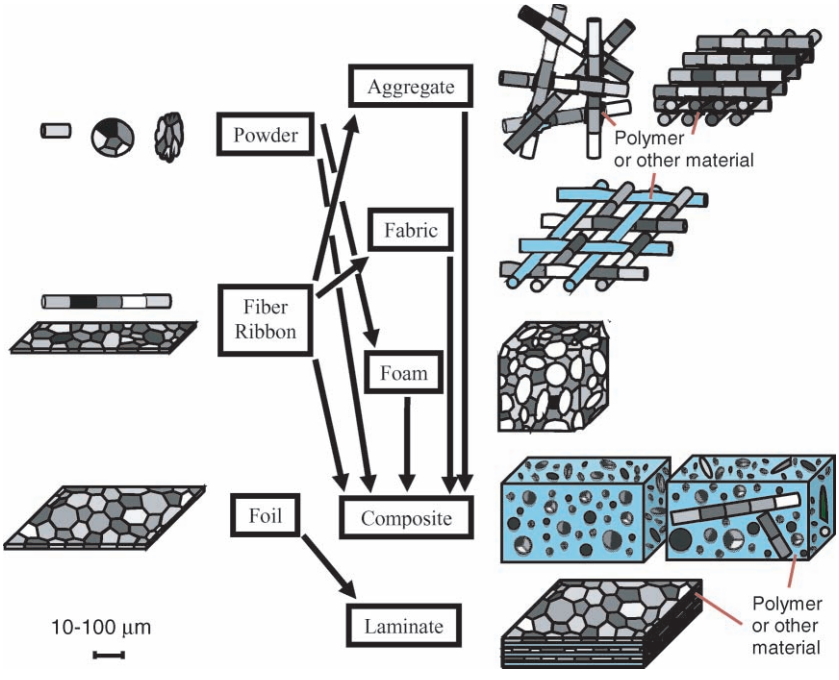

Figure 1. Schematic showing for Ni-Mn-Ga: (left) the various "elements" (powders, fibers, ribbon and films) with 1D or 2D geometries containing bamboo grains (spanning at least one dimension of the "element") with crystallographic orientations illustrated with various gray shades; (right) three-dimensional "constructs" (mats, foams, textiles, laminates and composites) using these elements as building blocks.

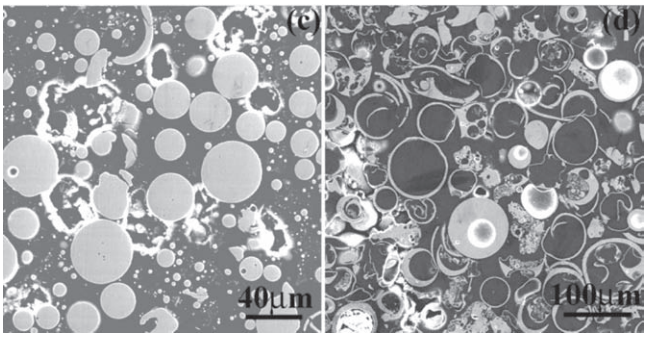

Figure 2. Polished cross-section of epoxy-embedded Ni-Mn-Ga particles produced by spark-erosion in (a) liquid argon (full particles) and (b) liquid nitrogen (hollow particles). Reprinted with permission from [60]. Copyright 2004, American Institute of Physics.

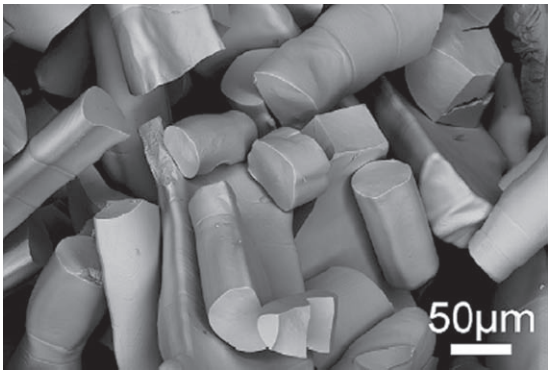

Figure 4. Short Ni–Mn–Ga fibers created by mortar grinding of longer fibers, composed of single or few grains spanning the fiber width. Reprinted with permission from [91]. Copyright 2007, Elsevier.

Mono- or oligo-crystalline powders are needed to achieve large MFIS. The simplest method capable of creating large quantities of such powders is based on crushing of bulk Ni-Mn-Ga with coarse grains (which are easily achievable by slow, directional solidification) or single crystal scrap (remaining after cutting operations). This simple powder production method takes advantage of the brittle nature of Ni-Mn-Ga and is thus similar to well established methods used for ceramic powder production. It is least likely to result in change of crystal structure (as in high-energy ball milling) or composition from chemical contamination and/or loss of alloying elements. Finer size Ni-Mn-Ga powders created by other methods tend to be polycrystalline, necessitating a grain growth annealing step, which may be difficult to carry out without concomitant partial sintering of the powders and/or composition changes from contamination or alloying element evaporation, exacerbated by the high surface to volume ratio.

2.2. Fibers and Ribbons

Unlike ductile alloys, brittle Ni-Mn-Ga cannot be cold-drawn to create fibers. Most researchers to date rely on melt spinning

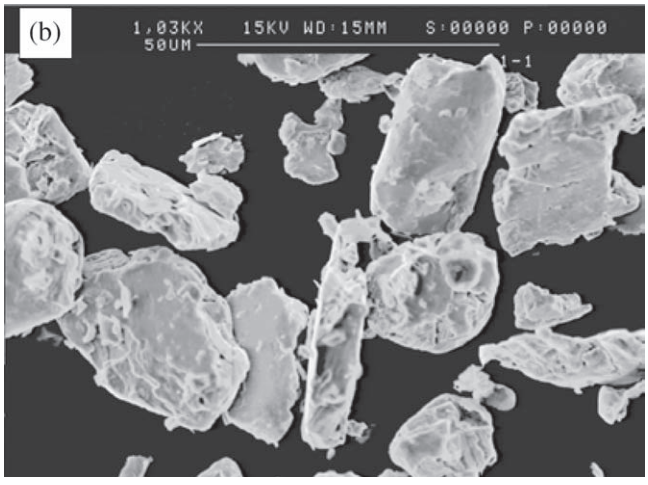

Figure 3. As-milled Ni-Mn-Ga particles. Reprinted with permission from [64]. Copyright 2007, the Royal Swedish Academy of Sciences.

(and the related melt extraction method) where the molten Ni-Mn-Ga is rapidly solidified onto a rotating copper wheel to form ribbons. Unlike fibers, ribbons have thicknesses (~10–100 μm) much smaller than their width (~1–10 mm), with lengths of 10–100 mm limited by fracture. Ribbons have been created by melt spinning from Ni-Mn-Ga[71–77] and other FSMA (e.g., Ni-Mn-Sn,[78] Ni-Mn-In,[79] Ni-Mn-In-Co,[80] Co-Ni-Al,[81] and Fe-based alloys[82–85]). Alternatively, the Taylor-Ulitovsky method, which has been used for many metals and alloys,[86] has been applied to Ni-Mn-Ga to create fine fibers with equiaxed cross-sections. In this method, the alloy is melted within a glass tube which is drawn rapidly into a fiber resulting in the solidification of the enclosed metal. Taylor wires have been reported with ~20 μm diameter within a 2–30 μm thick glass sheets (which can be removed by cracking of the glass) for Ni-Mn-Ga,[84] and with 24 μm diameter and 5 μm glass coating for Cu-Ga-Mn.[87] Finally, thin Co-Ni-Ga rods (with 800 μm diameter and 4–6 cm length) were created by suction casting into molds,[84] but this method is discontinuous and limited to large diameter wires, and is thus only practical for small quantities.

In all three methods described above for Ni-Mn-Ga fibers or ribbons, solidification is both directional and rapid, leading to a fine grain structure with strong crystallographic texture. For example, an as-solidified 80 μm thick ribbon showed 1–3 μm large grains, which after annealing coarsened to a 40 μm size. These ribbons maintained a strong texture (i.e., <100> directions perpendicular to the ribbon plane) during annealing.[71] Equiaxed grains with ~20 μm size were reported in another study.[75] Texture may reduce incompatibility between grains during twinning, as shown in bulk Ni-Mn-Ga samples,[88] and may thus be beneficial for achieving high MFIS in textured ribbons. On the other hand, the as-cast grain size, which is much finer than the ribbon dimensions, is undesirable from the point of view of strain incompatibility between grains.

While field-induced twin boundary motion was reported from indirect measurements (hysteresis loops) in fine-grained Ni-Mn-Ga ribbons,[73] a vanishingly small MFIS (0.002%) was measured in fine-grained, as-cast ribbons under an applied magnetic field of 1 T.[74] Achieving grain sizes similar to the wire or ribbon cross-section will reduce constraints between neighboring grains deforming by twinning, and thus increase the MFIS. A step in that direction was achieved for a ribbon

whose MFIS (at 1 T) increased from 0.005% in the as-cast state to 0.025% in the annealed state, where grain growth was ascertained indirectly by a change in transformation temperature.[72] However, the MFIS dropped to 0.017% after 50 cycles, as a result of relaxation of internal stresses, as indirectly shown by the evolution of magnetization curves.[72] To achieve a bamboo grain structure (with single grains spanning the whole cross-section) in ribbons might be difficult given that their thickness is typically much smaller than the width: grains may span the whole thickness, but only part of the width of the ribbon, resulting in strain incompatibility between grains across the ribbon width. In fact, to date, no report exists on coarse-grained Ni-Mn-Ga ribbons.

Bamboo grains in metallic fibers with near equiaxed cross-section are easily achievable by annealing.[89,90] This was recently demonstrated in Ni-Mn-Ga by Scheerbaum et al.,[91,77] who reported that a melt-extracted fiber, with 60 μm diameter and 5 μm grain size, achieved a bamboo grain structure, with single grains spanning the whole fiber cross-section (see **Figure 5**), after annealing for 2 h at 1100 °C (very close to the solidus temperature of ~1120 °C[92]). Application of a 2 T magnetic field perpendicular and parallel to the annealed fiber resulted in a 1% MFIS measured over the whole fiber.[77,91] Because of the lack of texture, only a subset of grains was favorably oriented to show a detectable MFIS. For these individual grains, a large MFIS of ~6% was measured using electron backscatter diffraction and scanning electron microscopy and confirmed based on calculations considering the angle between the fiber axis and the grain crystallographic *c* axis. Thus, if the grains within a bamboo structured fiber can be optimally oriented such that they all exhibit MFIS, a further improvement by a factor 2–4 in the MFIS can probably be achieved, approaching the MFIS value of single-crystals (6–10%).

Other methods developed for brittle fibers could be applied for production of Ni-Mn-Ga fibers. First, since foils have been produced by hot rolling of a Ni-Mn-Ga ingot encapsulated within a ductile iron sleeve without cracking,[93] hot-drawing or -swaging of sleeved Ni-Mn-Ga ingots into wires or fibers may be successful. Second, the similar and well-established "powder-in-tube" method[94] could be used, where prealloyed powders (or a blend of elemental powders) are densified within a ductile metallic tube during a hot-drawing operation. The metallic sheath can then be removed chemically or electrochemically. For Ni-Mn-Ga, a possible variation could be to draw a blend of Mn and Ga powders (or prealloyed near-equiatomic Ga-Mn powders) within a hollow Ni tube, and then anneal to interdiffuse the elements to form the Ni_2MnGa phase. If Kirkendall porosity can be avoided, the resulting Ni-Mn-Ga fiber would be without sheath.

Third, solid freeform fabrication techniques developed for ceramics could be used for Ni-Mn-Ga, where powders suspended in thick inks are extruded through fine nozzles by robocasting,[95] ink-jet printing,[96] or micropen writing[97] before being sintered into fibers, or fibers arrays. Similarly, Ni-Mn-Ga fibers could be produced by local melting of prealloyed or elemental powders, as illustrated for other alloys with electron beams or lasers.[98,99] A fourth method used for brittle ceramic fibers is the growth of monocrystalline fibers from the melt,[100] which is however a slow method prone to composition drift in the case of Ni-Mn-Ga due to the high vapor pressure of Mn. Finally, ceramic fibers (C and SiC) are created by chemical vapor deposition on a heated metallic core fiber (e.g., W) and this method might be feasible for Ni-Mn-Ga. Here again, taking advantage of the high ductility of nickel, a fine Ni fiber could be used as substrate onto which Ni, Mn and Ga are deposited in the gas phase (via chemical or physical vapor deposition) and diffused at elevated temperature to create single-phase Ni-Mn-Ga. A challenge with gas phase deposition is to maintain the correct ratio between the elements being co-deposited. Better control can be achieved by electrodeposition which is attractive since Ni, Mn and Ga can all be electrodeposited.[101–103] Ni-Mn-Ga fibers could be produced continuously and economically by co-deposition[104] onto a very thin Ni wire, followed by annealing to create the intermetallic phase and simultaneously coarsen the grains. Alternatively, wires of binary Ni-33 at.% Mn or Ni-33 at.%Ga, if ductile enough for wire drawing, could be used. The above methods could also be used to create films and foils.

2.3. Pillars

Deformation of monocrystalline pillars of various face-centered and body-centered-cubic materials has been extensively studied using compression tests, see e.g. refs. [53–55,105]. These materials exhibit a strong size dependence of the flow stress (controlled by dislocations), which increases with decreasing size. For a monocrystalline Ti alloy, the stress required for deformation twinning increased strongly with decreasing pillar sizes, until dislocation motion was the sole deformation mechanism at submicron sizes.[106,107] The superelastic behavior of sub-micron NiTi pillars deforming by twinning was also found to be highly dependent on diameter but only weakly on orientation.[108] Decreasing sample size reduced stress-strain hysteresis, with loss of recoverable superelastic strain for diameters below 200 nm.[109] In contrast, pillars of a Cu-Al-Ni shape-memory alloy showed superelastic and shape-memory behavior with complete shape recovery at both the micro- and nanometer scales,[110] a result confirmed with microwires with bamboo grains.[89,90]

Ganor et al.[56] showed a more than doubling of the blocking stress from 5 to >11 MPa

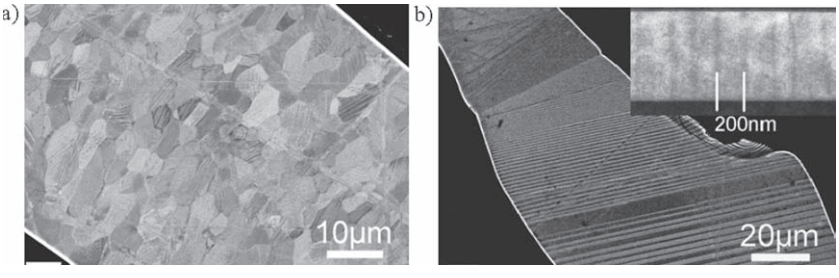

Figure 5. Cross-sections of melt-extracted Ni-Mn-Ga fibers (a) before annealing, with ~5 μm grains some of which are heavily twinned and (b) after annealing, with large bamboo grains containing twins spanning the fiber diameter. Reprinted with permission from [91]. Copyright 2007, Elsevier.

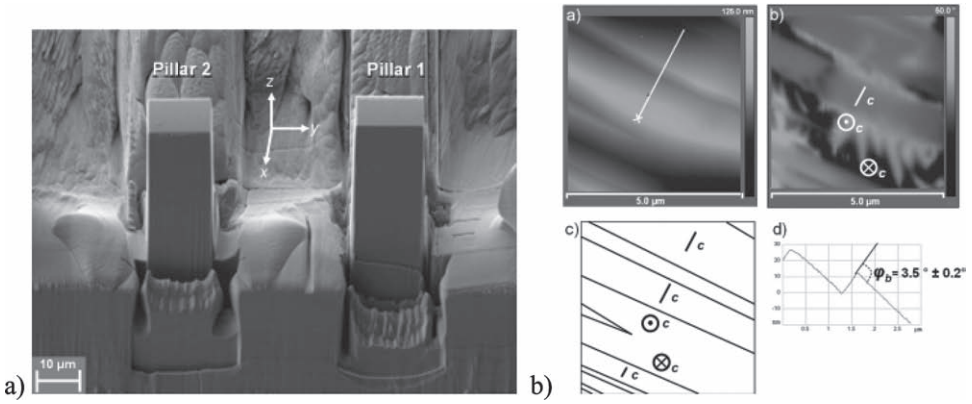

Figure 6. Ni-Mn-Ga micropillars. (a) after fabrication by focused ion beam. (b) Twins revealed by surface relief in the atomic force microscope (top left in b), and by the phase contrast in the magnetic force microscope (top right in b). Bottom left and right in (b) are a schematic of the twin pattern and a profile along the white line in the AFM image (top left in b). Reprinted with permission from [111]. Copyright 2009, American Institute of Physics.

when reducing the size of Ni-Mn-Ga single crystals to a square 200 μm × 200 μm cross-section. At the largest applied bias stress of 11 MPa, the MFIS obtained with the small sized crystal was still close to 2%. To the authors knowledge, there is to date only one study reporting deformation experiments of Ni-Mn-Ga micropillars.[111] While the very low force needed to trigger twinning of these 10 μm × 15 μm cross-section pillars presented a challenge for detecting twinning events at the onset of the deformation experiments, twinning was found to occur at quite large stress levels (~50 MPa) which may however be due to sample preparation. Post-deformation atomic force and magnetic force microscopy study confirmed the formation of twins (**Figure 6**).

Various levels of MFIS were found for Ni-Mn-Ga bilayers. For 0.1–1 μm thick Ni-Mn-Ga films on a 10 μm thick Mo substrate, an MFIS of up to 0.065% was reported.[114,115] Interestingly, the largest MFIS was obtained for the thinnest (0.1 μm) of all films on Mo. Ohtsuka et al.[116] found an MFIS of close to 0.04% for 5 μm thick Ni-Mn-Ga films on 14 μm polyvinyl alcohol (PVA) substrates. Due to the bimaterial effect, large deflections can be obtained in bilayers as a result of magnetic-field-induced and thermally induced martensitic transformations. A 2D optical scanner making use of bilayers of Ni-Mn-Ga on PVA was demonstrated in ref. [117].

For thin plates (10 mm × 6 mm × 2 mm) which were directionally solidified so that the elongated grains had diameters comparable to the plate thickness, MFIS values of up to 0.16%

2.4. Films

Processes including the synthesis of free standing films and beams are reviewed in Section 3.1. Film properties including texture, stress, stress distribution, grain size, phase transformation, magnetic properties, and the thickness dependence of these properties are also described in Section 3.1. Here, the discussion is limited to the description of MFIS in thin films, which was so far reported only for free standing films and bilayers.

Bernard et al.[112] measured the deflection of free-standing cantilevers fabricated with focused ion beam from films deposited on Si wafers (**Figure 7**). An MFIS of 0.025% was obtained after annealing the films at 600 °C for 10 hours. This was a ten-fold increase compared to the MFIS of cantilevers fabricated from films deposited on substrates which were at 600 °C during deposition. For films peeled from the substrate and annealed, Bernard et al.[112] demonstrated a magnetic-field-induced curling and de-curling due to MFIS (but uniaxial MFIS was not measured). No magnetic response was found for as-deposited and peeled films, an effect attributed to the lack of order in as-deposited films. Jenkins et al.[113] demonstrated that strains in cantilevers fabricated from Ni-Mn-Ga films (Figure 7) are produced by the magnetic-field-induced motion of twin boundaries.

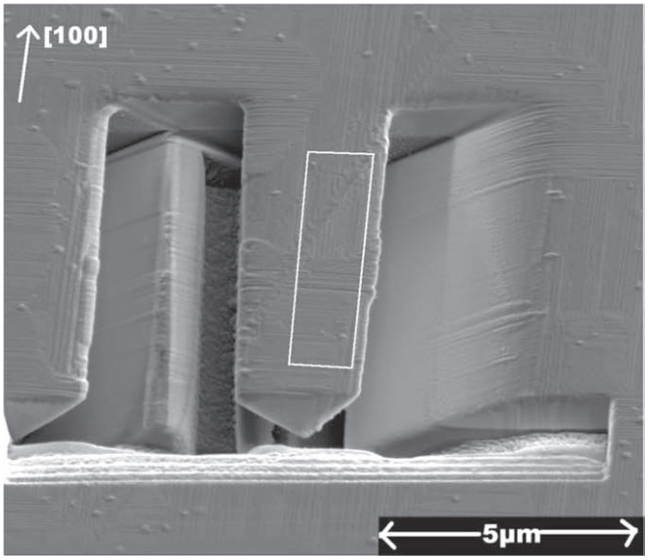

Figure 7. Ni-Mn-Ga micro-cantilevers with a triangular cross-section, cut with an ion beam from films grown epitaxially on MgO. The twin boundaries moved in response to a magnetic field demonstrating MFIS. Reprinted with permission from [113]. Copyright 2008, American Institute of Physics.

have been obtained; by contrast, a more equi-axed parallelepiped sample with all edges much larger than the grain size did not deform in a magnetic field.[118] For a macroscopic bicrystal (which may be considered the transition case between an oligocrystal and a single crystal), a strong mechanical training effect reduced the twinning stress to values below twice the magnetostress implying that large MFIS is possible (see Section 1.2 and Equation (3)).[119]

3. Three-dimensional Aggregates and Constructs

Fibers, ribbons and films are 1D and 2D objects which can be used individually in miniature devices (e.g. actuators and sensors). For macroscopic devices, these could be assembled into bulk 3D structures, with or without magnetically induced alignment, as illustrated in Figure 1 and further described below:

(i) *Bonded powder beds (or short fiber mats)*, where bonding occurs at contact points between powders (or short fibers) at elevated temperature by sintering, with or without additional solder or liquid phase sintering aids, or at low temperature with adhesives or by electro-deposition. The construct maintains an open porosity with the individual shape of the Ni-Mn-Ga powder/fibers recognizable. If sintering is extensive, a cellular or sponge-like structure may result, as demonstrated for shape-memory NiTi.[120]

(ii) *Woven, braided, and knitted fabrics*, where continuous Ni-Mn-Ga fibers, alone or together with non shape-memory fibers (e.g. polymers), are interwoven into a textile without inter-fiber bonding, as demonstrated with shape-memory NiTi fibers.[121–124]

(iii) *Composites and laminates*, where all the space between the powders/fibers (for composites) and films (for laminates) is filled by a matrix, which is polymeric (for composites) but may be non polymeric for laminates.

Of the above 3D architectures, laminates, composites and foams have been implemented for Ni-Mn-Ga and are reviewed and discussed below.

3.1. Laminates

3.1.1. Film Fabrication

Ni-Mn-Ga films can be fabricated by various deposition methods, the most commonly used being direct current (DC) and radio frequency (RF) magnetron sputtering [125], most often with a single alloyed target (rather than multiple elemental targets). To study the influence of film composition – particularly the effect of quaternary elements – multiple sputter targets are required. Koike et al.[126] and Ohtsuka et al.[127] used two targets, with the first providing the Ni-Mn-Ga base composition and the second the fourth pure element (Fe or Co). This set-up allowed to systematically varying the Fe and Co contents while keeping the ratios of Ni, Mn, and Ga constant. The main experimental parameters for sputtering are the sputtering power, the argon back pressure, and the substrate temperature. Cai et al.[128] found for Ni-Fe-Ga films that, with increasing sputtering power, the film composition becomes richer in Fe and Ga, and depleted in Ni. The substrate temperature impacts texture, grain size, ordering, and magnetic properties, as further described in more detailed below. Castaño et al.[129] reported an increase of the Mn content with increasing substrate temperature. Increasing argon pressure and decreasing sputtering power increased the residual film stresses.[112]

Less commonly, molecular beam epitaxy (MBE) has been applied for MSMA films.[130] Hassdorf et al.[131] studied the Ni-Mn-Al phase diagram in a combinatorial approach using elemental sources. While combinatorial studies provide ample information, including the stability range of the martensite phase and ferromagnetic ordering, the substrate constrains the films, thus shifting phase boundaries. Further Ni-Mn-Ga film fabrication methods include pulsed laser deposition,[132,133] laser beam ablation,[134] flash evaporation of alloy powders,[135] and multi-dipolar plasma-assisted sputtering, which may be performed with multiple alloy targets.[136]

When deposited at room temperature, Ni-Mn-Ga films are mostly nanocrystalline or even amorphous. Post-deposition annealing leads to significant grain growth resulting in mostly columnar grain structures (**Figure 8**[125,137]). Wu et al.[138] found a crystallization energy of 234 kJ/mol (2.3 eV/atom) for amorphous Ni-Mn-Ga films deposited on Si(100). For Ni-Mn-Ga, grain sizes from the nanometer range[139] to several micrometers were reported.[125] Liu et al.[140] found grain sizes ranging from 0.5 to 2 μm in free standing Ni-Mn-Ga films. These films were first sputtered on aluminum foils, then peeled off and annealed at 650 °C. To reduce constraints resulting from grain boundaries, which would allow for large MFIS, the grain size should be much larger than the film thickness. Typically, grain growth is limited by grain boundary pinning at surface grooves[141] so that the grain size is limited to about twice the film thickness. This seems to be also the case for Ni-Mn-Ga.[125]

Finally, Ni-Mn-Ga foils can be produced by hot-rolling at temperatures where the B2 structure is stable (>770 ºC) and the alloy deforms plastically in compression. For example, a polycrystalline rod with 7 × 7 × 40 mm dimensions was encapsulated within an iron sleeve and hot rolled at 1000 ºC into a 1.2 × 12 × 130 mm foil without cracking;[93] foils with sub-millimeter thicknesses are probably achievable with this method. Crystallographic texture as a result of Ni-Mn-Ga hot-rolling to ~80% was reported,[142] which will likely improve MFIS values.

3.1.2. Substrates

The Ni-Mn-Ga film properties depend on the choice of substrate material. The substrates found in the literature may be classified in three groups: (A) single crystalline hard substrates; (B) polycrystalline and amorphous hard substrates (these include single crystalline substrates with an amorphous surface layer or a buffer layer); and (C) compliant substrates. The properties of the films further depend strongly on the substrate temperature where, as a rule, increasing substrate temperature produces a higher degree of structural and magnetic order in the deposited Ni-Mn-Ga film.

Ni-Mn-Ga grows epitaxially on various monocrystalline surfaces including GaAs,[130] MgO(100),[113] yttria-stabilized zirconia

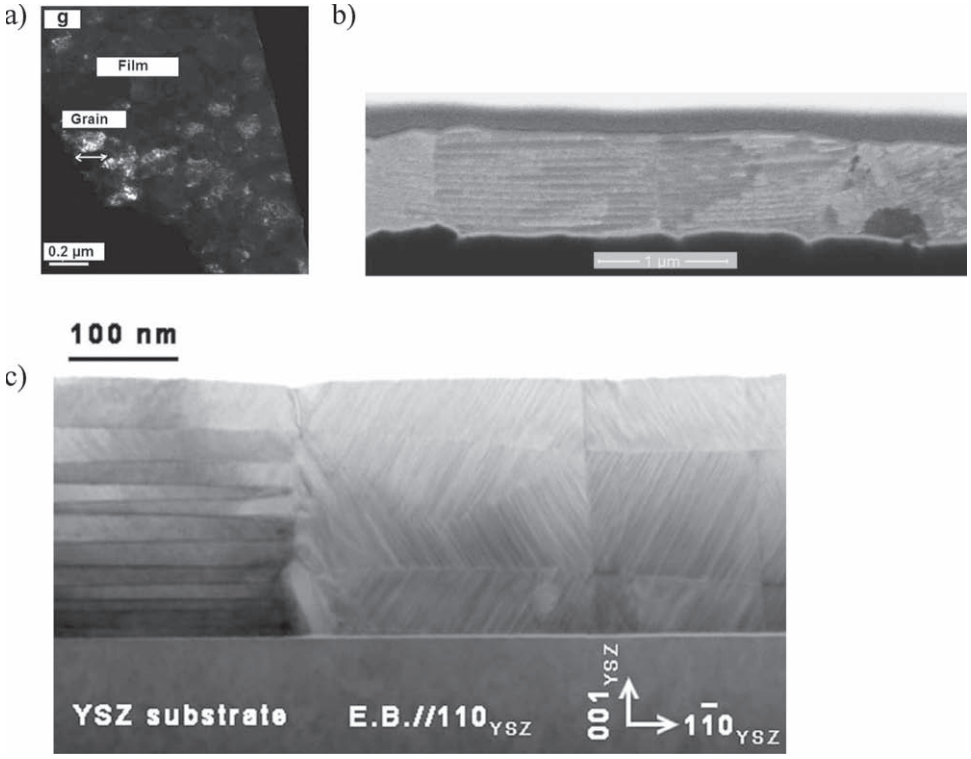

Figure 8. Ni-Mn-Ga thin films. (a) TEM cross-section of a polycrystalline film on Si with grain size smaller than film thickness. Reprinted with permission from [112]. Copyright 2009, Elsevier. (b) FIB cross-section of a polycrystalline film with a strong 110 texture and grain size larger than the film thickness. Reprinted with permission from [125]. Copyright 2006, The Japan Institute of Metals. (c) TEM cross-section of epitaxial films with martensite domain variants on YSZ substrate. Reprinted with permission from [163]. Copyright 2010, The American Physical Society.

(YSZ(100),[143] $SrTiO_3$,[144] and Al_2O_3(110).[145,146] Because of the low stiffness of Ni-Mn-Ga, films can be grown epitaxially with rather large crystallographic misfit with the substrate. The elastic compliance also enables growing films epitaxially when sputtered,[146] which allows growing oriented films much faster than with MBE. Epitaxial films can be grown in $(100)_{film}$[147] and $(110)_{film}$[143] orientation. Chernenko et al.[148] demonstrated three epitaxial orientation relationships for Ni-Mn-Ga films on MgO(100), which depended on film thickness (varied from 30 nm to 1 μm), including (100) planes parallel to the film surface, which would lead to the highest MFIS.

The most prominent representative of group B substrates is monocrystalline silicon wafers cut along (100) with a native oxide layer which prevents interdiffusion between Ni-Mn-Ga and Si and suppresses interfacial reaction, i.e., the formation of silicides.[133,112] To enhance these functions, an additional diffusion barrier may be grown on the Si(100) wafer before depositing the film. Golub et al.[149] have used silicon nitride for that purpose. Other group B substrates include polycrystalline alumina,[125,150] 100 μm thick aluminum foil,[140] 10 μm thick molybdenum foil,[114] glass,[134] and mica.[135] When the substrate is actively cooled during deposition, the Ni-Mn-Ga films on these substrates are nano-crystalline or even amorphous. When the substrate is heated during deposition, grains grow during deposition and a strong 110 fiber texture evolves.

Polymer substrates include polyvinyl alcohol (PVA)[116] and photoresist.[151] The large compliance of these substrates allows for deposition of rather thick Ni-Mn-Ga films: Kohl et al.[117] grew 10 μm thick films on PVA. At this thickness, films would peel from stiff substrates because of significant film stresses and limited adhesion. The tendency to peel can be utilized for the fabrication of free-standing films.

3.1.3. Freestanding Films

Constraints imposed by the film/substrate interface cause significant stresses in the film (several hundred MPa[112]) which can suppress MFIS entirely. For magneto-mechanical devices as sensors and actuators, the substrate thus needs to be removed. Free standing films have been produced by first depositing films on various substrates including glass,[152] aluminum,[140] silicon,[112] and photoresist.[151] In a second step, these films were peeled from the substrate. An alternative route makes use of a sacrificial layer such as chromium, which can be removed by etching[153] or a sacrificial substrate such as NaCl, which can be dissolved.[154] In both cases, it is possible to fabricate single crystalline films via epitaxy.

Dong et al.[130] produced free-standing cantilevers and bridges from epitaxial monocrystalline films with (100) parallel to the substrate by using standard photolithography and reactive ion etching. They fabricated rectangular bridges measuring 100 μm × 400 μm with the edges parallel to <110> and cantilevers 100 μm long and 25 μm wide. Bridges and cantilevers exhibited the conventional shape-memory effect and magnetic-field-induced twin boundary motion,[113] which indicates a potential for large MFIS.

3.1.4. Texture

When grown on heated substrates and when annealed after deposition on cooled substrates, Ni-Mn-Ga films develop a strong 110 fiber texture. In some cases, a preferred in-plane orientation was reported.[155,156] The fiber texture is less pronounced in very thin films (~0.1 μm) and intensifies with increasing film thickness.[157] A strong 110 fiber texture also evolves during post deposition annealing (e.g., ref. [11]).

The thermal expansion coefficient of Ni-Mn-Ga is larger than that of most stiff substrates. The thermo-elastic mismatch leads to large tensile in-plane film stress. The film stress relaxes partially during the martensitic transformation.[158] The reduction of the tensile film stress favors those martensite variants, which have one of the crystallographic *a* directions parallel to the film plane. For the 110 textured films, this implies that the crystallographic *c* direction is preferentially oriented at 45° to the film normal.[159,149]

For simple actuator or sensor devices based on Ni-Mn-Ga thin films, the film geometry would require the use of a field perpendicular or parallel to the film plane. The magneto-mechanical response would be strongest for films with the crystallographic *c* direction parallel or perpendicular to the film plane and, thus, 100 textured films would be most advantageous. Hakola et al.[133] reported the formation of such a 100 texture for Ni-Mn-Ga films deposited via laser ablation on a heated GaAs(100) substrate with a buffer layer.

The formation of a given texture is the result of the interplay between surface (and interface) energy and strain energy density.[137] The surface energy is independent of film thickness whereas the total strain energy is proportional to the film thickness. Therefore, very thin films tend to develop a texture which minimizes the surface energy leading to closed packed planes being parallel to the film surface. This controls the 110 fiber texture in Ni-Mn-Ga films. Very thick films tend to develop a texture which minimizes the strain energy. The low value of the C' modulus ($C' = (C_{11} - C_{12})/2$), i.e., the large shear compliance on the {110} plane in <110> direction, would favor a 100 fiber texture. Typically, strain energy controlled textures form at higher annealing temperatures and for films deposited on substrates with large thermoelastic mismatch.[137] Thus, one strategy to fabricate Ni-Mn-Ga films with 100 texture would be to anneal thick films on stiff substrates with low thermal expansion coefficient at high temperature. Another strategy might be to seek conditions for abnormal grain growth, which might lead to a texture transformation, as demonstrated for silver films.[160]

3.1.5. Magnetic-field-induced Reorientation of Martensite

Partial magnetic-field-induced reorientation (MIR) of twin variants was demonstrated for epitaxial Ni-Mn-Ga films with 14 M orthorhombic martensite on MgO(100) and $SrTiO_3$.[144,113,161,162] The reorientation of martensite variants was inferred from the shape of the magnetic hysteresis loops and confirmed by X-ray texture measurements.[161] Here, the martensite variants with the crystallographic *b* direction parallel to the applied field grew at the expense of the variants with the crystallographic *a* and *c* directions parallel to the magnetic field. The driving force of this process is attributed to a reduction of the total magnetic anisotropy energy, because the saturation field along the crystallographic *b* direction is less than the average of the saturation fields along the *a* and *c* directions. This process, however, does not result in a significant MFIS because the lattice parameter *b* is close to the average of the lattice parameters *a* and *c*. From an analytical model it was concluded that the volume fraction of *b*-variants increased from 1/3 to ~0.5.[161]

In very recent studies,[143,163] MIR was demonstrated for epitaxial Ni-Mn-Ga films with 14 M martensite on yttria stabilized zirconia, YSZ(100), substrates. These films were grown in the austenite phase with a (110) $[001]_{aust}//(001)[110]_{substrate}$ orientation relationship. The austenite phase exists in two orientation variants with $[001]_{aust}$ parallel to $[110]_{substrate}$ and $[1\bar{1}0]_{substrate}$, respectively. Upon cooling, each austenite orientation variant transforms into two twin-related martensite variants with a $(101)[010]_{aust}//(001)[110]_{substrate}$ orientation relationship. For all martensite variants, the twin boundaries are (101) and they are parallel to the substrate (Figure 8c). Therefore, the twin boundaries can move without imposing a strain on the substrate which does not obstruct twin-boundary motion. The magnetic field was applied in the $[110]_{substrate}$ direction, which caused the twins in one orientation variant (referring to the austenite variants) becoming active whereas the twins in the other orientation variants stayed inactive. The inactive variants do not respond to the magnetic field and, hence, generate a restoring force on the active variants, which leads to a "self-activation of the reversible MIR effect".

In the study by Zhang et al.,[163] large MFIS was suppressed by the existence of inactive martensite variants. This hindrance might be easily overcome by utilizing micro-fabrication techniques (e.g., focused-ion-beam milling) to isolate active domains from inactive ones and cutting micro- or nano-pillars. These pillars would then tilt under the action of a magnetic field by an angle given by the twinning shear.

Thomas et al.[154] recently discovered stray-field-induced shape memory as a new actuation mechanism. This mechanism uses the temperature as actuation field but is intrinsically different from the conventional two-way shape memory effect as it does not require training. Instead, the stray field of the martensite phase controls the fractions of martensite variants with the crystallographic *c* direction parallel and perpendicular to the film plane, respectively. Thus, the shape anisotropy of thin films enables stray-field-induced shape memory. The formation of 180° domains reduces the shape anisotropy. As suggested by Thomas et al.[154], a single domain state may be approached for very thin films, in which case the stray field would be fully developed. This would imply a size effect where the stray-field-induced shape memory effect gets stronger with decreasing film thickness and device size.

3.1.6. Film Stress

The majority of stresses in thin films result from the interaction with the substrate. Origins are found in the thermo-elastic mismatch (i.e., the difference of the thermal expansion coefficients of substrate and film), densification processes in the film during deposition and during grain growth, and phase transformations. Film stresses can be measured with X-ray diffraction with the "$\sin^2\psi$-method", or with the substrate curvature method.[164]

Bernard et al.[112] found stresses ranging from –600 to +800 MPa in Ni-Mn-Ga films on Si(100) and a stress gradient of up to 300 MPa across the film in peeled-off films. The film stress increased strongly when deposited at larger Ar back pressure and decreased with increasing deposition power. The stress variation during the martensitic phase transformation can be measured with the substrate curvature method.[159] Hassdorf et al.[131] measured stress variations of up to 400 MPa for Ni-Mn-Al films.

Doyle et al.[165] found that the Ni-Mn-Ga film stress increases with decreasing film thickness for Si and MgO substrates and film thickness <1 μm. This trend was found with the $\sin^2\psi$-method and with the substrate curvature method.[157] The inverse dependence of stress on film thickness is typical for metal films on stiff substrates.[164,166] The opposite dependence, i.e., decreasing film stress with decreasing film thickness, was found for Ni-Mn-Ga films on polycrystalline Al_2O_3 ceramics substrate.[165] These substrates have surface corrugations which induce localized shear stress concentrations in the films. Shear stresses due to surface roughness induce martensite in NiTi films,[167] and probably do the same in Ni-Mn-Ga films. Thus, the stress concentrations trigger the martensitic transformation which, in turn, reduces the average film stress detected with the substrate curvature measurement.

3.1.7. Martensite Phase Transformation Temperature

The martensite transformation temperature was found to increase with decreasing film thickness for Ni-Mn-Ga films on alumina ceramics[165] and for 14 M martensite on Si(100) substrates.[11] The opposite trend was found for 10 M martensite on Si(100) substrates and for epitaxial films on sapphire, particularly near the surface.[168] Some of the results regarding thickness dependence of the transformation temperature appear to be contradictory, which may be related to effects of texture and film stress. There is a trend that the transformation temperature increases with decreasing film thickness for films for which the film stress decreases with decreasing film thickness.[165] For films with the inverse thickness dependence of film stress, the transformation temperature decreases with decreasing film thickness.[169,125,170] The apparent contradiction of the results may also originate from different thickness dependencies of the effects of surface roughness and texture on the onset of the martensitic transformation, which can facilitate or obstruct the transformation.[167,171]

3.1.8. Magnetic Properties

Besides magnetocrystalline anisotropy, shape anisotropy plays a significant role in MSMA thin films. In most reported cases, the films magnetize more easily in-plane than out-of-plane. This is the case for most substrates, e.g., Mo,[114] GaAs,[130] mica,[135] and Si(100).[172,149] The magnetic anisotropy can be measured with a standard vibrating sample magnetometer[172] and with ferromagnetic resonance (FMR) experiments.[135,149] Chernenko et al.[172] measured magnetization curves of Ni-Mn-Ga films on alumina substrates at various angles between magnetic field and film normal. Golub et al.[149] studied the orientation dependence of magnetic properties of films on Si(100) with FMR. Both studies found that the magnetostatic energy, which controls the shape anisotropy, turns the magnetic moments away from the crystallographic easy axis towards the plane of the films with 110 texture. For the film on silicon, the FMR study showed that the uniaxial anisotropy constant increases with increasing film thickness. Unlike single crystals, which have an easy axis/hard plane anisotropy, films have an easy plane/hard axis anisotropy. These studies show that one needs to distinguish between overall magnetic anisotropy, which most often is controlled by the shape anisotropy and the magnetocrystalline anisotropy which is at 45° for 110 textured films.[149]

The magnetic domain structure, particularly the size of magnetic domains, may critically impact the magneto-mechanical properties of small size structures.[56,154] Magnetic force microscopy studies revealed magnetic domain pattern of the maze type for films on MgO(100),[156] polycrystalline alumina,[173] and molybdenum foils.[114] For all these films, the domain size decreased with decreasing film thickness, where the relationship between domain width δ and film thickness d was approximated as $\delta \sim d^{1/2}$. Venkateswaran et al.[174,175] studied the magnetic domain patterns of thin foils with Lorentz TEM microscopy. They found maze domain structures as well as domains which are aligned with crystallographic planes. In the latter case, 90° domain boundaries coincide with twin boundaries and 180° domain boundaries are parallel to the (100) planes (**Figure 9**).

In two cases only, Ni-Mn-Ga laminates have been produced. In a first article which does not report on magnetomechanical properties,[176] two architectures were created: (i) a laminate consisting of twenty layers of Ni-Mn-Ga ribbons glued with epoxy and (ii) a sandwich, consisting of three monocrystalline

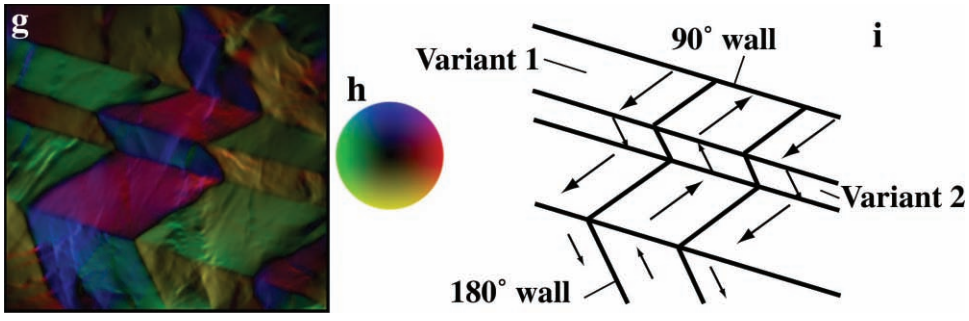

Figure 9. Lorentz TEM image of magnetic domains in Ni-Mn-Ga thin foil (left), orientation key (center) and schematic with the directions of the magnetic moments (right). The edge of the left image measures about 2.5 μm. Reprinted with permission from [174]. Copyright 2007, Elsevier.

Ni-Mn-Ga plates bonded with two internal layers of epoxy. A second report[177] describes sandwiches with polyurethane faces and (i) a core consisting of a 1-mm thick monocrystalline Ni-Mn-Ga plate or (ii) two monocrystalline Ni-Mn-Ga rods (~1 mm × 2 mm cross-section). These sandwiches exhibited a MFIS of 1%, significantly less than the 4.9% value for the unbonded single crystal, which was justified by a rule-of-mixture calculation considering the back-stress acting on the Ni-Mn-Ga elements from the elastically deformed polymer.

3.2. Composites

All studies of Ni-Mn-Ga composites to date consider polymer matrices containing Ni-Mn-Ga particles (rather than fibers), produced by spark erosion,[59,61,178,179] mechanical alloying,[68] crushing of ingots,[59,63,180] and crushing of fibers or ribbons.[69,70,91] The polymer matrices used in these studies are epoxy,[63,68,176,180] polyester,[69,70,91] polyurethane,[59,61,178,179] and silicone, [176] and good bonding is reported in most cases.[176] Most studies use field alignment of the particles by curing the composite under an externally applied magnetic field.[59,61,63,68,69,91,178,180,179] Particles then form aligned chains within the matrix, which optimizes the response of the composite to a magnetic field by enhancing the shape anisotropy. However, alignment of particles into chains also facilitates cracking of the composites.[180] The observed magnetic anisotropy in the composites indicates that the powders themselves show some crystallographic texture.[68] The total magnetic anisotropy results from the shape anisotropy – which may be strong in aligned powder chains – and from the magnetocrystalline anisotropy – which may be strong in single crystalline powders or textured polycrystalline powders.

The majority of the Ni-Mn-Ga composite studies focused on the damping and energy absorption properties, which are enhanced by the strain-induced twinning of the Ni-Mn-Ga reinforcement.[59,61,176,178,179] Indirect evidence of twinning during composite deformation was provided by change in magnetic properties with compressive strain[59,69,70,91,178] while direct evidence was given by texture changes measured by X-ray diffraction[61,70] and neutron diffraction.[179]

A simple model predicting the MFIS for Ni-Mn-Ga composites provides an upper limit value of strain as 21% of the MFIS of a bulk single crystal for randomly oriented particles and 50% for field-aligned particles.[181] A 3D models based on composite theory provides MFIS predictions for various particle shape, applied stress, and matrix stiffness. Optimal MFIS in the Ni-Mn-Ga composite are predicted for the following parameters: matrix stiffness of 0.1 GPa; spherical or rod-like Ni-Mn-Ga particles with axis of rotation corresponding to the easy axes of the crystal; magnetic field applied along this same direction; biasing stress aligned to disfavor variants favored by the magnetic field.[181] A 2D numerical model based on elastic and magnetic field energies explores various parameters for Ni-Mn-Ga/polymer composites.[182,183] Conclusions are that magnetic orientation of the particles in the composite is more important than their alignment, that optimal work output is achieved with elongated rather than equiaxed particles, which must be somewhat stiffer than the matrix.[182,183]

Experimentally, however, no value of MFIS are reported for Ni-Mn-Ga/polymer composites, despite the fact that some of these composites contained mono- or oligo-crystalline powders (from crushed fibers with bamboo grains)[69,91] which were field aligned. In one case,[91] this lack of MFIS was assigned to the high stiffness of the polyester matrix used. Decreasing polymer matrix fraction and stiffness (e.g., using elastomers) and introducing porosity in the composites (as discussed in the next section for foams) may lead to Ni-Mn-Ga composites capable of high MFIS. Another approach is to use aligned, continuous Ni-Mn-Ga fibers, or even an open porosity Ni-Mn-Ga foam infiltrated by a polymer to create an interpenetrating-phase composite (as achieved in another material system[184]).

3.3. Foams and Cellular Ni-Mn-Ga

Metallic foams can display a large range of architectures and microstructures[185]. For Ni-Mn-Ga foams to exhibit large MFIS, porosity is introduced to reduce constraints imposed by grain boundaries and to form bamboo grains. This was recently achieved in replicated foams which were produced by infiltration of liquid Ni-Mn-Ga into a bed of sodium aluminate space-holder powders. After solidification the space-holder was removed by etching to create porosity[186]. These foams consist of large bamboo grains with twins spanning the full width of the struts (**Figure 10**). Each grain behaves like a single crystal with high MFIS, similar to bamboo grains in Ni-Mn-Ga fibers.[77,91] The struts are constrained by polycrystalline nodes limiting the overall MFIS of the foam to 0.12%.[186] Introducing fine porosity within the nodes (**Figure 11**) further reduced constraints during twinning and dramatically increased MFIS to

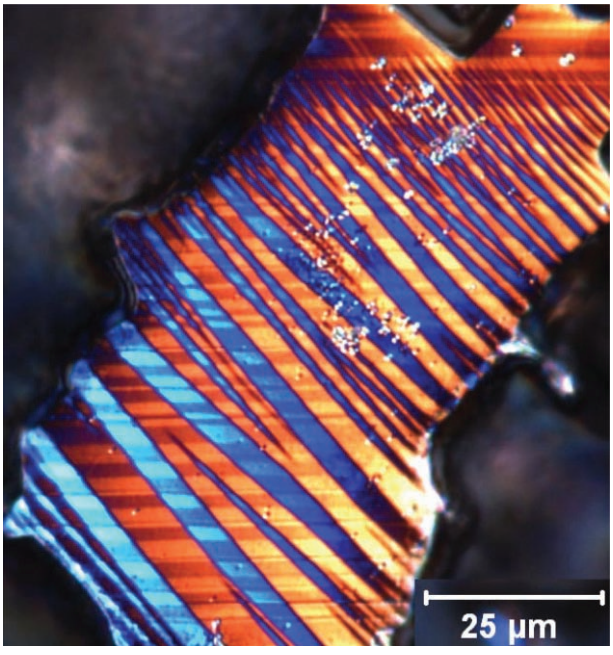

Figure 10. Cross-section of strut in Ni-Mn-Ga foam with twins spanning the width of the strut within a single bamboo grain. Reprinted with permssion from [19]. Copyright 2009, Nature Publishing Group.

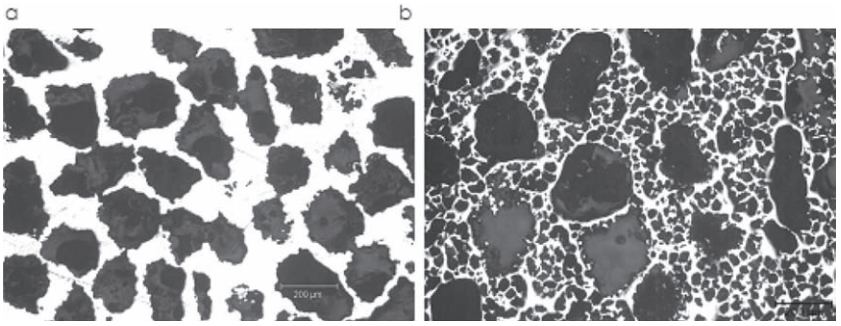

Figure 11. Cross-section of Ni-Mn-Ga foams produced by replication of $NaAlO_2$ powders with a) medium 355–500 µm pores and (b) coarse 500–600 µm pores and fine 75–90 µm pores. Image from X. X. Zhang, P. Müllner, and D. C. Dunand, previously unpublished.

2.0-8.7%, these values remaining stable over >**200 000** strain cycles (**Figure 12**[19]). The 8.7% MFIS value exceeds the average strain calculated for a collection of isolated, unconstrained monocrystalline struts, which indicates that (i) the foam is textured, because of solidification and/or (ii) geometrical effects, such as plastic hinging of the struts due to a magnetic-field-induced torque, may be operative.[187]

Novel foam architectures may be achievable in Ni-Mn-Ga by applying existing processing methods for other metallic foams.[185] For example, a foam could be created by densifying via hot-pressing a blend of monocrystalline or coarse-grained Ni-Mn-Ga powders or short fibers and space-holder powders (e.g. NaF, as used previously for NiTi foams[188]). The space-holder phase is then dissolved from the resulting composite, creating a foam with well controlled pore size, shape, fraction and connectivity; alternatively, the space-holder can decompose or evaporate during a pressureless sintering step, as also demonstrated for NiTi.[188] Also, sintering of hollow Ni-Mn-Ga powders, which have been created by spark erosion in liquid nitrogen,[60] would create a syntactic foam, as demonstrated with other metallic hollow spheres.[189,190] Another possible method relies on the expansion in the solid state of pressurized argon bubbles entrapped during a previous powder densification step, as recently achieved for NiTi foams.[191] For the above powder-metallurgy methods, if the Ni-Mn-Ga powder particles are magnetically aligned before densification, a foam with highly textured grains can be produced. Finally, closed porosity can be achieved by solidifying a melt of Ni-Mn-Ga containing gas bubbles, as demonstrated for various low melting metallic foams.[185] An alternate method is to deposit Mn and Ga (by PVD or CVD) onto the struts of commercially-available Ni foams to achieve after interdiffusion the Ni-Mn-Ga composition, as demonstrated by CVD addition of Al and Cr to Ni-foams.[192]

Complex 3-D periodic architectures (e.g., arrays of parallel rods arranged in a regular stack to form a tower-like structure) have been produced from gel-based inks containing ceramic particle suspensions by fused deposition or direct-write methods.[95,193,194] This method could be used for Ni-Mn-Ga powders, followed by sintering (and interdiffusion if elemental powders are used) and annealing to achieve bamboo grains. Similarly, periodic structures consisting of a lattice of struts created by successive sintering or melting of layers of powders by laser or electron beam (as demonstrated for, e.g., titanium[98,195]) could be implemented for Ni-Mn-Ga.

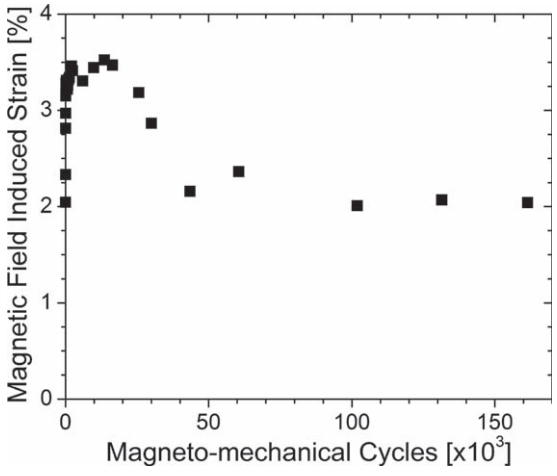

Figure 12. Plot of MFIS vs. magneto-mechanical cycles for a Ni-Mn-Ga foam with bamboo grains and bimodal pore size distribution subjected to a rotating field of 1 T. Reprinted with permission from [19]. Copyright 2009, Nature Publishing Group.

4. Conclusions and Outlook

In monocrystalline form, the magnetic shape-memory alloy Ni-Mn-Ga deforms to high strains (up to 10%) by the motion of twin boundaries driven by a magnetic field. This MFIS can be used for actuation purpose (with rapid response rates and millions of reversible strain cycles) and for magnetomechanical actuation and sensing. The high cost of growing monocrystalline Ni-Mn-Ga and strong tendency for chemical segregation during crystal growth make polycrystalline, cast Ni-Mn-Ga desirable, but their MFIS is near zero due to constraints during twinning of neighboring grains.

Oligocrystalline Ni-Mn-Ga, where grains are grown such that their size becomes comparable to one or more characteristic sample sizes, are expected to reduce these constraints between neighboring grains and thus raise the MFIS of polycrystalline Ni-Mn-Ga close to that of monocrystalline Ni-Mn-Ga. When grain boundaries are replaced by a surface, twinning disconnections are no longer blocked but are free to escape through the surface. Thus, disconnections do not form pile-ups and the disconnection sources continue to be operative at a low stress level while deformation via twin boundary motion proceeds. This approach has been demonstrated very recently for Ni-Mn-Ga fibers[77,91] and foams with grains having bamboo-like structure[19] as well as for thin plates with thickness similar to grain diameter[118] and for a macroscopic bicrystal.[119]

In other words, free surfaces act as sinks for twinning disconnections and allow for stress relaxation between grains. Both effects enable MFIS and are, thus, important not only for

polycrystalline materials with large surface to volume ratio. Even in bulk single crystals, large MFIS is obtained only in well-trained crystals, in which twin boundaries extend from surface to surface across the entire crystal and are not blocked by differently oriented twin variants.[38,196]

When the grain size (e.g. in a strut or fiber) becomes small in one or two dimensions, additional effects arise. Small size obstructs the formation of dislocations and very likely also the formation of twinning disconnections. For very pure single-domain single crystals, the twinning stress is controlled by nucleation.[38] A similar effect is likely to occur at small length scales. Consequently, one would expect an increase of the twinning stress with decreasing size (i.e. with decreasing strut or fiber diameter or film thickness), which would hinder MFIS.

A second effect is related to an increase of the magnetic anisotropy with decreasing sample size.[56] This effect, which was attributed to a hindrance of magnetization rotation, increases the blocking stress, which promotes MFIS. Thus, size effects are both inhibiting and promoting MFIS. Which effect ultimately dominates is a question which is still open. To this end, fundamental studies will be important for advancing magnetic shape-memory alloys for small size applications.

In recent years, significant progress has been made in the fabrication of Ni-Mn-Ga powders, fibers, ribbons and films. These elements, after annealing to grow grains with dimensions comparable to the element to display large MFIS, could be assembled into various "constructs" (mats, laminates, textiles, foams and composites) with large MFIS as well. Such microstructurally and architecturally tailored materials may displace existing monocrystalline Ni-Mn-Ga for rapid actuators, and expand or even create new magneto-mechanical and other applications ranging from micro-valves to smart dampers harvesting vibration energy.

Acknowledgements

The authors thank Ms. Peiqi Zheng (Northwestern University) for assistance with generating Figure 1 and acknowledge the financial support of the National Science Foundation through grants DMR-805064 (Northwestern University) and DMR 0804984 (Boise State University).

Received: July 30, 2010
Published online: October 19, 2010

[1] K. Ullakko, J. K. Huang, C. Kantner, R. C. O'Handley, *Applied Phys. Lett.* **1996**, *69*, 1966.
[2] J. Ma, I. Karaman, *Science* **2010**, *327*, 1468.
[3] P. Müllner, G. Kostorz, *Mater. Sci. Forum* **2008**, *583*, 43.
[4] A. Nespoli, S. Besseghini, S. Pittaccio, E. Villa, S. Viscuso, *Sens. Actuators A* **2010**, *158*, 149.
[5] V. A. Chernenko, V. A. L'vov, P. Müllner, G. Kostorz, T. Takagi, *Phys. Rev. B* **2004**, *69*, 134410.
[6] P. Müllner, V. A. Chernenko, G. Kostorz, *Scr. Mater.* **2003**, *49*, 129.
[7] I. Karaman, B. Basaran, H. E. Karaca, A. I. Karsilayan, Y. I. Chumlyakov, *Appl. Phys. Lett.* **2007**, *90*, 172505.
[8] *Shape Memory Materials* (Eds: K. Otsuka, C. M. Wayman), Cambridge **1998**.
[9] K. A. Gschneidner, V. K. Pecharsky, A. O. Tsokol, *Reports on Progress in Physics* **2005**, *68*, 1479.
[10] H. E. Karaca, I. Karaman, B. Basaran, Y. Ren, Y. I. Chumlyakov, H. J. Maier, *Adv. Funct. Mater.* **2009**, *19*, 983.
[11] V. A. Chernenko, M. Ohtsuka, M. Kohl, V. V. Khovailo, T. Takagi, *Smart Mater. Struct.* **2005**, *14*, S245.
[12] G. Kostorz, P. Müllner, *Z. Metallkunde* **2005**, *96*, 703.
[13] V. A. Chernenko, *Adv. Mater. Res.* **2008**, *52*, 3.
[14] O. Söderberg, I. Aaltio, Y. Ge, O. Heczko, S. P. Hannula, *Mater. Sci. Eng. A* **2008**, *481*, 80.
[15] O. Söderberg, I. Aaltio, Y. L. Ge, X. W. Liu, S. P. Hannula, *State-of-the-Art Research and Application of Smas Technologies* **2009**, *59*, 1.
[16] U. Gaitzsch, M. Pötschke, S. Roth, B. Rellinghaus, L. Schultz, *Acta Mater.* **2009**, *57*, 365.
[17] H. A. Das, F. H. M. Spit, *J. Radioanal. Nucl. Chem. Lett.* **1987**, *117*, 171.
[18] D. Raabe, *Metall. Mater. Trans.* **1994**, *181*, 291.
[19] M. Chmielus, X. X. Zhang, C. Witherspoon, D. C. Dunand, P. Müllner, *Nat. Mater.* **2009**, *8*, 863.
[20] M. A. Marioni, R. C. O'Handley, S. M. Allen, *Appl. Phys. Lett.* **2003**, *83*, 3966.
[21] E. Arzt, *Acta Mater.* **1998**, *46*, 5611.
[22] Y. Tanaka, Y. Himuro, R. Kainuma, Y. Sutou, T. Omori, K. Ishida, *Science* **2010**, *327*, 1488.
[23] R. C. O'Handley, *J. Appl. Phys.* **1998**, *83*, 3263.
[24] J. P. Hirth, R. C. Pond, *Acta Mater.* **1996**, *44*, 4749.
[25] R. C. Pond, S. Celotto, *Intl. Mater. Rev.* **2003**, *48*, 225.
[26] J. M. Howe, R. C. Pond, J. P. Hirth, *Prog. Mater. Sci.* **2009**, *54*, 792.
[27] T. E. Mitchell, J. P. Hirth, *Acta Metall. Mater.* **1991**, *39*, 1711.
[28] Y. Q. Sun, P. M. Hazzledine, J. W. Christian, *Phil. Mag. A* **1993**, *68*, 471.
[29] Y. Q. Sun, P. M. Hazzledine, J. W. Christian, *Phil. Mag. A* **1993**, *68*, 495.
[30] P. Müllner, *Z. Metallkunde* **2006**, *97*, 205.
[31] A. E. Romanov, A. L. Kolesnikova, *Prog. Mater. Sci.* **2009**, *54*, 740.
[32] P. Müllner, V. A. Chernenko, M. Wollgarten, G. Kostorz, *J. Appl. Phys.* **2002**, *92*, 6708.
[33] H. E. Karaca, I. Karaman, B. Basaran, Y. J. Chumlyakov, H. J. Maier, *Acta Mater.* **2006**, *54*, 233.
[34] N. Okamoto, T. Fukuda, T. Kakeshita, *Mater. Sci. Eng. A* **2008**, *481*, 306.
[35] J. J. Rhyne, S. Foner, E. J. Mcniff, R. Doclo, *J. Appl. Phys.* **1968**, *39*, 892.
[36] H. H. Liebermann, C. D. Graham, *Acta Metall.* **1977**, *25*, 715.
[37] R. D. James, M. Wuttig, *Phil. Mag. A* **1998**, *77*, 1273.
[38] L. Straka, N. Lanska, K. Ullakko, A. Sozinov, *Appl. Phys. Lett.* **2010**, *96*, 131903.
[39] A. Sozinov, A. A. Likhachev, K. Ullakko, *Proc. SPIE* **2001**, *4333*, 189.
[40] A. Sozinov, A. A. Likhachev, N. Lanska, K. Ullakko, *Appl. Phys. Let.* **2002**, *80*, 1746.
[41] A. Sozinov, A. A. Likhachev, K. Ullakko, *IEEE Trans. Magn.* **2002**, *38*, 2814.
[42] O. Heczko, L. Straka, *J. Appl. Phys.* **2003**, *94*, 7139.
[43] O. Heczko, L. Straka, V. Novak, S. Fähler, *J. Appl. Phys.* **2010**, *107*, 09A914.
[44] V. A. Chernenko, J. Pons, C. Segui, E. Cesari, *Acta Mater.* **2002**, *50*, 53.
[45] S. Rajasekhara, P. J. Ferreira, *Scr. Mater.* **2005**, *53*, 817.
[46] K. Otsuka, T. Ohba, M. Tokonami, C. M. Wayman, *Scr. Metall. Mater.* **1993**, *29*, 1359.
[47] N. A. Stelmashenko, M. G. Walls, L. M. Brown, Y. V. Milman, *Acta Metall. Mater.* **1993**, *41*, 2855.
[48] A. C. Fischer-Cripps, *Nanoindentation,* Springer, New York 2004.
[49] N. A. Fleck, G. M. Muller, M. F. Ashby, J. W. Hutchinson, *Acta Metall. Mater.* **1994**, *42*, 475.
[50] J. S. Stolken, A. G. Evans, *Acta Mater.* **1998**, *46*, 5109.

[51] C. Motz, T. Schoberl, R. Pippan, *Acta Mater.* **2005**, *53*, 4269.
[52] G. Dehm, *Prog. Mater. Sci.* **2009**, *54*, 664.
[53] J. R. Greer, W. D. Nix, *Phys. Rev. B* **2006**, *73*, 245410.
[54] C. A. Volkert, E. T. Lilleodden, *Phil. Mag. A* **2006**, *86*, 5567.
[55] D. Kiener, W. Grosinger, G. Dehm, R. Pippan, *Acta Mater.* **2008**, *56*, 580.
[56] Y. Ganor, D. Shilo, T. W. Shield, R. D. James, *Appl. Phys. Lett.* **2008**, *93*, 122509.
[57] J. Liu, N. Scheerbaum, O. Gutfleisch, *IEEE Trans. Magn.* **2008**, *44*, 3025.
[58] J. Liu, N. Scheerbaum, S. Weiss, O. Gutfleisch, *Appl. Phys. Let.* **2009**, *95*, 152503.
[59] J. Feuchtwanger, S. Michael, J. K. Juang, D. Bono, R. C. O'Handley, S. M. Allen, C. Jenkins, J. Goldie, A. Berkowitz *J. Appl. Phys.* **2003** *93* 8528.
[60] V. C. Solomon, D. J. Smith, Y. Tang, A. E. Berkowitz, *J. Appl. Phys.* **2004**, *95*, 6954.
[61] J. Feuchtwanger, M. L. Richard, Y. J. Tang, A. E. Berkowitz, R. C. O'Handley, S. M. Allen, *J. Appl. Phys.* **2005**, *97*, 10M319.
[62] V. C. Solomon, M. R. McCartney, D. J. Smith, Y. Tang, A. E. Berkowitz, R. C. O'Handley, *Appl. Phys. Lett.* **2005**, *86*, 192503.
[63] H. Hosoda, S. Takeuchi, T. Inamura, K. Wakashima, *Sci. Technol. Adv. Mater.* **2004**, *5*, 503.
[64] F. Chen, B. Tian, L. Li, Y. Zheng, *Phys. Scr.* **2007**, *T129*, 227.
[65] D. M. Liu, Z. H. Nie, Y. D. Wang, Y. D. Liu, G. Wang, Y. Ren, L. Zuo, *Metall. Mater. Trans.* **2008**, *39*A, 466.
[66] B. Tian, F. Chen, Y. Liu, Y. F. Zheng, *Intermetallics* **2008**, *16*, 1279.
[67] B. Tian, F. Chen, Y. Liu, Y. F. Zheng, *Mater. Lett.* **2008**, *62*, 2851.
[68] T. D. Hatchard, J. S. Thorne, S. P. Farrell, R. A. Dunlap, *J. Phys.: Condensed Matter* **2008**, *20*, 445205.
[69] D. Hinz, N. Scheerbaum, O. Gutfleisch, K. H. Müller, L. Schultz, *J. Magn. Magn. Mater.* **2007**, *310*, 2785.
[70] N. Scheerbaum, D. Hinz, O. Gutfleisch, *J. Appl. Phys.* **2007**, *101*, 09C501.
[71] O. Heczko, P. Svec, D. Janickovic, K. Ullakko, *IEEE Trans. Magn.* **2002**, *38*, 2841.
[72] S. H. Guo, Y. H. Zhang, B. Y. Quan, J. L. Li, X. L. Wang, *PRICM 5: the Fifth Pacific Rim International Conference on Advanced Materials and Processing, Pts. 1-5 (Materials Science Forum)* **2005**, *475–479*, 2009.
[73] J. Gutierrez, J. M. Barandiaran, P. Lazpita, C. Seguí, E. Cesari, *Sens. Actuators A* **2006**, *129*, 163.
[74] P. Lazpita, G. Rojo, J. Gutierrez, J. M. Barandiaran, R. C. O'Handley, *Sensor Lett.* **2007**, *5*, 65.
[75] A. K. Panda, M. Ghosh, A. Kumar, A. Mitra, *J. Magn. Magn. Mater.* **2008**, *320*, L116.
[76] A. K. Panda, A. Kumar, M. Ghosh, A. Mitra, *J. Magn. Magn. Mater.* **2008**, *320*, E730.
[77] N. Scheerbaum, O. Heczko, J. Liu, D. Hinz, L. Schultz, O. Gutfleisch, *New J. Phys.* **2008**, *10*, 073002.
[78] B. Hernando, J. L. S. Llamazares, J. D. Santos, L. Escoda, J. J. Sunol, R. Varga, J. Gonzalez, *Appl. Phys. Lett.* **2008**, *92*, 042504.
[79] B. Hernando, J. L. S. Llamazares, J. D. Santos, M. L. Sanchez, L. Escoda, J. J. Sunol, R. Varga, C. Garcia, J. Gonzalez, *J. Magn. Magn. Mater.* **2009**, *321*, 763.
[80] J. Liu, T. G. Woodcock, N. Scheerbaum, O. Gutfleisch, *Acta Mater.* **2009**, *57*, 4911.
[81] Z. H. Liu, X. F. Dai, Z. Y. Zhu, H. N. Hu, J. L. Chen, G. D. Liu, G. D. Wu, *J. Phys. D: Appl. Phys.* **2004**, *37*, 2643.
[82] T. Todaka, M. Szpryngacz, M. Enokizono, I*ntl. J. Appl. Electromagn. Mech.* **2004**, *19*, 149.
[83] T. Todaka, T. Yasuoka, M. Enokizono, K. Tsutsumi, R. Groessinger, R. S. Turtelli, C. Bormio-Nunes, G. Wiesinger, *J. Magn. Magn. Mater.* **2006**, *304*, E516.
[84] C. M. Craciunescu, A. Ercuta, I. Mitelea, M. Valeanu, V. S. Teodorescu, N. Lupu, H. Chiriac, *Eur. Phys. J.* **2008**, *158*, 161.
[85] V. M. Prida, V. Vega, V. Franco, J. L. S. Llamazares, M. J. Perez, J. D. Santos, L. l. Escoda, J. J. Sunol, B. Hernando, *J. Magn. Magn. Mater.* **2009**, *321*, 790.
[86] I. W. Donald, B. L. Metcalfe, *J. Mater. Sci.* **1996**, *31*, 1139.
[87] C. Garcia, V. M. Prida, V. Vega, J. L. S. Llamazares, J. J. Sunol, L. Escoda, M. L. Sanchez, J. Ribot, B. Hernando, *Phys. Status Solidi A* **2009**, *206*, 644.
[88] T. Liang, C. B. Jiang, H. B. Xu, Z. H. Liu, M. Zhang, Y. T. Cui, G. H. Wu, *J. Magn. Magn. Mater.* **2004**, *268*, 29.
[89] G. Khatibi, R. Stickler, V. Groger, B. Weiss, *J. Alloys Compd.* **2004**, *378*, 326.
[90] Y. Chen, X. X. Zhang, D. C. Dunand, C. A. Schuh, *Appl. Phys. Lett.* **2009**, *95*, 171906.
[91] N. Scheerbaum, D. Hinz, O. Gutfleisch, K. H. Muller, L. Schultz, *Acta Mater.* **2007**, *55*, 2707.
[92] D. L. Schlagel, Y. L. Wu, W. Zhang, T. A. Lograsso, *J. Alloys Compd.* **2000**, *312*, 77.
[93] S. Besseghini, E. Villa, F. Passaretti, M. Pini, F. Bonfanti, *Mater. Sci. Eng. A* **2004**, *378*, 415.
[94] A. Godeke, A. den Ouden, A. Nijhuis, H. H. J. ten Kate, *Cryognenics* **2008**, *48*, 308.
[95] J. E. Smay, G. M. Gratson, R. F. Shepherd, J. Cesarano, J. A. Lewis, *Adv. Mater.* **2002**, *14*, 1279.
[96] K. A. M. Seerden, N. Reis, J. R. G. Evans, P. S. Grant, J. W. Halloran, B. Derby, *J. Am. Ceram. Soc.* **2001**, *84*, 2514.
[97] S. L. Morissette, J. A. Lewis, P. G. Clem, J. Cesarano, D. B. Dimos, *J. Am. Ceram. Soc.* **2001**, *84*, 2462.
[98] D. A. Hollander, M. von Walter, T. Wirtz, R. Sellei, B. Schmidt-Rohlfing, O. Paara, H. J. Erli, *Biomaterials* **2006**, *27*, 955.
[99] L. E. Murr, S. M. Gaytan, F. Medina, E. Martinez, J. L. Martinez, D. H. Hernandez, B. I. Machado, D. A. Ramirez, R. B. Wicker, *Mater. Sci. Eng. A* **2010**, *527*, 1861.
[100] P. Rudolph, T. Fukuda, *Cryst. Res. Technol.* **1999**, *34*, 3.
[101] C. L. Mantell, *J. Electrochem. Soc.* **1948**, *94*, 232.
[102] J. D. Corbett, *J. Electrochem. Soc.* **1962**, *109*, 1214.
[103] P. Ilea, I. C. Popescu, M. Urda, L. Oniciu, *Hydrometallurgy* **1997**, *46*, 149.
[104] N. Atanassov, V. Mitreva, *Surf. Coatings Technol.* **1996**, *78*, 144.
[105] M. D. Uchic, D. A. Dimiduk, *Mater. Sci. Eng. A* **2005**, *400*, 268.
[106] O. Kraft, *Nat. Mater.* **2010**, *9*, 295.
[107] Q. Yu, Z. Shan, J. Li, X. Huang, L. Xiao, J. Sun, E. Ma, *Nature* **2010**, *463*, 335.
[108] C. P. Frick, B. G. Clark, S. Orso, P. Sonnweber-Ribic, E. Arzt, *Scr. Mater.* **2008**, *59*, 7.
[109] C. P. Frick, S. Orso, E. Arzt, *Acta Mater.* **2007**, *55*, 3845.
[110] J. M. S. Juan, M. L. No, C. A. Schuh, *Adv. Mater.* **2008**, *20*, 272.
[111] M. Reinhold, D. Kiener, W. B. Knowlton, G. Dehm, P. Müllner, *J. Appl. Phys.* **2009**, *106*, 053906.
[112] F. Bernard, P. Delobelle, C. Rousselot, L. Hirsinger, *Thin Solid Films* **2009**, *518*, 399.
[113] C. A. Jenkins, R. Ramesh, M. Huth, T. Eichhorn, P. Pörsch, H. J. Elmers, G. Jakob, *Appl. Phys. Lett.* **2008**, *93*, 234101.
[114] V. A. Chernenko, R. L. Anton, M. Kohl, J. M. Barandiaran, M. Ohtsuka, I. Orue, S. Besseghini, *Acta Mater.* **2006**, *54*, 5461.
[115] M. Kohl, A. Agarwal, V. A. Chernenko, M. Ohtsuka, K. Seemann, *Mater. Sci. Eng. A* **2006**, *438*, 940.
[116] M. Ohtsuka, M. Matsumoto, K. Koike, T. Takagi, K. Itagaki, *J. Magn. Magn. Mater.* **2007**, *310*, 2782.
[117] M. Kohl, D. Brugger, M. Ohtsuka, B. Krevet, *Sens. Actuators A* **2007**, *135*, 92.
[118] M. Pötschke, S. Weiss, U. Gaitzsch, D. Cong, C. Hürrich, S. Roth, L. Schultz, *Scr. Mater.* **2010**, *63*, 383.

[119] R. Chulist, W. Skrotzki, C.-G. Oertel, A. Böhm, M. Pötschke, *Scr. Mater.* **2010**, *63*, 548.
[120] A. Bansiddhi, D. C. Dunand, *J. Mater. Res.* 2009, *24*, 2107.
[121] C. M. Smyth, S. E. J. Edmunds, *J. Gastroenterol. Hepatol.* **2006**, *21*, A249.
[122] H. Van Der Merwe, B. D. Reddy, P. Zilla, D. Bezuidenhout, T. Franz, *J. Biomech.* **2008**, *41*, 1302.
[123] F. Ahlhelm, R. Kaufmann, D. Ahlhelm, M. F. Ong, C. Roth, W. Reith, *Cardiovascular and Interventional Radiology* **2009**, *32*, 1019.
[124] E. Villa, S. Arnaboldi, A. Tuissi, M. Giacomelli, E. Turco, *J. Mater. Eng. Perf.* **2009**, *18*, 517.
[125] V. A. Chernenko, M. Kohl, V. A. L'vov, V. M. Kniazkyi, M. Ohtsuka, O. Kraft, *Mater. Trans.* **2006**, *47*, 619.
[126] K. Koike, M. Ohtsuka, Y. Honda, H. Katsuyama, M. Matsumoto, K. Itagaki, Y. Adachi, H. Morita, *J. Magn. Magn. Mater.* **2007**, *310*, E996.
[127] M. Ohtsuka, M. Matsumoto, K. Itagaki, *Mater. Sci. Eng. A* **2006**, *438*, 935.
[128] W. Cai, H. B. Wang, X. An, L. X. Gao, Z. Y. Gao, L. C. Zhao, *Mater. Sci. Eng. A* **2006**, *438*, 994.
[129] F. J. Castano, B. Nelson-Cheeseman, R. C. O'Handley, C. A. Ross, C. Redondo, F. Castano, *J. Appl. Phys.* **2003**, *93*, 8492.
[130] J. W. Dong, J. Q. Xie, J. Lu, C. Adelmann, C. J. Palmstrom, J. Cui, Q. Pan, T. W. Shield, R. D. James, S. McKernan, *J. Appl. Phys.* **2004**, *95*, 2593.
[131] R. Hassdorf, J. Feydt, S. Thienhaus, R. Borowski, M. Boese, T. Walther, M. Moske, Combinatorial Thin Film Synthesis of NiMnAl Magnetic Shape Memory Alloys Using MBE Technique. *MRS Symposium on Materials and Devices for Smart Systems*, Boston, PA, Materials Research Society, Warrendale, PA., **2003**, p. 57–64.
[132] V. O. Golub, A. Y. Vovk, L. Malkinski, C. J. O'Connor, Z. J. Wang, J. K. Tang, *J. Appl. Phys.* **2004**, *96*, 3865.
[133] A. Hakola, O. Heczko, A. Jaakola, T. Kajava, K. Ullakko, *Appl. Surf. Sci.* **2004**, *238*, 155.
[134] C. Y. Chung, V. A. Chernenko, V. V. Khovailo, J. Pons, E. Cesari, T. Takagi, *Mater. Sci. Eng. A* **2004**, *378*, 443.
[135] J. Dubowik, Y. V. Kudryavtsev, Y. P. Lee, *J. Appl. Phys.* **2004**, *95*, 2912.
[136] G. Girard, S. Bechu, N. Caillault, L. Carbone, L. Ortega, D. Fruchart, *J. Alloys Compd.* **2008**, *465*, 35.
[137] C. V. Thompson, *Ann. Rev. Mater. Sci.* **2000**, *30*, 159.
[138] S. K. Wu, K. H. Tseng, J. Y. Wang, *Thin Solid Films* **2002**, *408*, 316.
[139] A. Vovk, L. Malkinski, V. Golub, C. O'Connor, Z. J. Wang, J. K. Tang, *J. Appl. Phys.* **2005**, *97*, 10C503.
[140] C. Liu, Z. Y. Gao, X. An, M. Saunders, H. Yang, H. B. Wang, L. X. Gao, W. Cai, *J. Magn. Magn. Mater.* **2008**, *320*, 1078.
[141] W. W. Mullins, *Acta Metall.* **1958**, *6*, 414.
[142] B. Lu, H. B. Wang, Y. Liu, J. X. Liu, H. L. Wang, *Trans. Nonferrous Metals Soc. China* **2006**, *16*, 843.
[143] Y. Zhang, R. A. Hughes, J. F. Britten, W. Gong, J. S. Preston, G. A. Botton, M. Niewczas, *Smart Materials & Structures* **2009**, *18*, 025019.
[144] O. Heczko, M. Thomas, J. Buschbeck, L. Schultz, S. Fähler, *Appl. Phys. Lett.* **2008**, *92*, 072502.
[145] G. Jakob, T. Eichhorn, M. Kallmayer, H. J. Elmers, Martensite transition and microscopic magnetism of epitaxial Ni2MnGa films, *MRS Symposium "Magnetic Shape Memory Alloys"*, Boston, MA, Materials Research Society, Warrendale, PA., 2007, p. 1050-BB08-2.
[146] G. Jakob, H. J. Elmers, *J. Magn. Magn. Mater.* **2007**, *310*, 2779.
[147] J. Buschbeck, R. Niemann, O. Heczko, M. Thomas, L. Schultz, S. Fahler, *Acta Mater.* **2009**, *57*, 2516.
[148] V. A. Chernenko, V. Golub, J. M. Barandiaran, O. Y. Salyuk, F. Albertini, L. Righi, S. Fabbrici, M. Ohtsuka, *Appl. Phys. Lett.* **2010**, *96*, 042502.
[149] V. Golub, K. M. Reddy, V. Chernenko, P. Müllner, A. Punnoose, M. Ohtsuka, *J. Appl. Phys.* **2009**, *105*, 07A942.
[150] V. Recarte, J. I. Perez-Landazabal, V. Sanchez-Alarcos, V. A. Chernenko, M. Ohtsuka, *Appl. Phys. Lett.* **2009**, *95*, 141908.
[151] J. Tillier, D. Bourgault, B. Barbara, S. Pairis, L. Porcar, P. Chometon, D. Dufeu, N. Caillault, L. Carbone, *J. Alloys Compd.* **2010**, *489*, 509.
[152] H. Rumpf, C. Craciunescu, J. Feydt, A. Gilles, M. Wuttig, E. Quandt, Fabrication and Characterization of Freestanding NiMnGa Films, *MRS Symposium "Materials and Devices for Smart Systems"*, Boston, MA, Materials Research Society, Warrendale, PA. **2003**, Vol. *785*, p. 195–199.
[153] A. Backen, S. R. Yeduru, M. Kohl, S. Baunack, A. Diestel, B. Holzapfel, L. Schultz, S. Fähler, *Acta Mater.* **2010**, *58*, 3415.
[154] M. Thomas, O. Heczko, J. Buschbeck, Y. W. Lai, J. McCord, S. Kaufmann, L. Schultz, S. Faehler, *Adv. Mater.* **2009**, *21*, 3708.
[155] V. A. Chernenko, S. Doyle, M. Kohl, P. Müllner, S. Besseghini, M. Ohtsuka, *Z. Kristallography Suppl.* **2007**, *26*, 229.
[156] V. A. Chernenko, R. L. Anton, J. M. Barandiaran, I. Orue, S. Besseghini, M. Ohtsuka, A. Gambardella, *IEEE Trans. Magn.* **2008**, *44*, 3040.
[157] S. Besseghini, A. Gambardella, V. A. Chernenko, M. Hagler, C. Pohl, P. Müllner, M. Ohtsuka, S. Doyle, *Eur. Phys. J.- Special Topics* **2008**, *158*, 179.
[158] A. L. Roytburd, T. S. Kim, Q. M. Su, J. Slutsker, M. Wuttig, *Acta Mater.* **1998**, *46*, 5095.
[159] M. Hagler, V. A. Chernenko, M. Ohtsuka, S. Besseghini, P. Müllner *MRS Symposium 'Nanoscale Magnetics and Device Applications'*, San Francisco, CA, Materials Research Society, Warrendale, PA **2008**, *998*, 0998-J06-09.
[160] J. Greiser, P. Müllner, E. Arzt, *Acta Mater.* **2001**, *49*, 1041.
[161] M. Thomas, O. Heczko, J. Buschbeck, U. K. Rössler, J. McCord, N. Scheerbaum, L. Schultz, S. Faehler, *New J. Phys.* **2008**, *10*, 023040.
[162] M. Thomas, O. Heczko, J. Buschbeck, L. Schultz, S. Fahler, *Appl. Phys. Lett.* **2008**, *92*, 192515.
[163] Y. P. Zhang, R. A. Hughes, J. F. Britten, J. S. Preston, G. A. Botton, M. Niewczas, *Phys. Rev. B* **2010**, *81*, 054406.
[164] W. D. Nix, *Metall. Trans. A - Phys. Metall. Mater. Sci.* **1989**, *20*, 2217.
[165] S. Doyle, V. A. Chernenko, S. Besseghini, A. Gambardella, M. Kohl, P. Müllner, M. Ohtsuka, *Eur. Phys. J.- Special Topics* **2008**, *158*, 99.
[166] B. von Blanckenhagen, E. Arzt, P. Gumbsch, *Acta Mater.* **2004**, *52*, 773.
[167] M. Wuttig, Y. Zheng, J. Slutsker, K. Mori, Q. M. Su, *Scr. Mater.* **1999**, *41*, 529.
[168] P. Pörsch, M. Kallmayer, T. Eichhorn, G. Jakob, H. J. Elmers, C. A. Jenkins, C. Felser, R. Ramesh, M. Huth, *Appl. Phys. Lett.* **2008**, *93*, 022501.
[169] V. Chernenko, M. Kohl, S. Doyle, P. Müllner, M. Ohtsuka, *Scr. Mater.* **2006,** *54*, 1287.
[170] V. A. Chernenko, M. Kohl, M. Ohtsuka, T. Takagi, V. A. L'vov, V. M. Kniazkyi, *Mater. Sci. Eng. A* **2006**, *438*, 944.
[171] H. T. Hesemann, P. Müllner, O. Kraft, E. Arzt, *J. Physique IV* **2003**, *112*, 107.
[172] V. A. Chernenko, M. Hagler, P. Müllner, V. M. Kniazkyi, V. A. L'vov, M. Ohtsuka, S. Besseghini, *J. Appl. Phys.* **2007**, *101*, 053909.
[173] V. A. Chernenko, R. L. Anton, M. Kohl, M. Ohtsuka, I. Orue, J. M. Barandiaran, *J. Phys.- Condens. Matter* **2005**, *17*, 5215.
[174] S. P. Venkateswaran, N. T. Nuhfer, M. De Graef, *Acta Mater.* **2007**, *55*, 5419.
[175] S. P. Venkateswaran, N. T. Nuhfer, M. De Graef, *Acta Mater.* **2007**, *55*, 2621.
[176] M. Lahelin, I. Aaltio, O. Heczko, O. Söderberg, Y. Ge, B. Lofgren, S. P. Hannula, J. Seppala, *Composites A* **2009**, *40*, 125.
[177] E. Gans, G. P. Carman, *J. Appl. Phys.* **2006**, *99*, 084905.

[178] J. Feuchtwanger, K. Griffin, J. K. Huang, D. Bono, R. C. O'Handley, S. M. Allen, *J. Magn. Magn. Mater.* **2004**, *272*, 2038.
[179] J. Feuchtwanger, P. Lazpita, N. Vidal, J. M. Barandiaran, J. Gutierrez, T. Hansen, M. Peel, C. Mondelli, R. C. O'Handley, S. M. Allen, *J. Phys.: Condens. Matter* **2008**, *20*, 104247.
[180] B. Tian, F. Chen, L. Li, Y. F. Zheng, *Mater. Lett.* **2007**, *17*, S630.
[181] M. A. Marioni, R. C. O'Handley, S. M. Allen, *J. Appl. Phys.* **2002**, *91*, 7807.
[182] S. Conti, M. Lenz, M. Rumpf, *J. Mech. Phys. Solids* **2007**, *55*, 1462.
[183] S. Conti, M. Lenz, M. Rumpf, *Mater. Sci. Eng. A* **2008**, *481–482*, 351.
[184] X. L. Gong, Y. Liu, S. Y. He, J. Lu, *J. Mater. Sci. Technol.* **2004**, *20*, 65.
[185] J. Banhart, *Progr. Mater. Sci.* **2001**, *46*, 559.
[186] Y. Boonyongmaneerat, M. Chmielus, D. C. Dunand, P. Müllner, *Phys. Rev. Lett.* **2007**, *99*, 247201.
[187] A. E. Markaki, T. W. Clyne, *Acta Mater.* **2005**, *53*, 877.
[188] A. Bansiddhi, D. C. Dunand, *Acta Biomater.* **2008**, *4*, 1996.
[189] T. J. Lim, B. Smith, D. L. McDowell, *Acta Mater.* **2002**, *50*, 2867.
[190] B. Neville, A. Rabiei, *Materials and Design* **2008**, *29*, 388.
[191] S. M. Oppenheimer, D. C. Dunand, *Mater. Sci. Eng. A* **2009**, *523*, 70.
[192] H. Choe, D. C. Dunand, *Acta Mater.* **2004**, *52*, 1283.
[193] J. E. Smay, J. Cesarano, J. A. Lewis, *Langmuir* **2002**, *18*, 5429.
[194] G. M. Gratson, M. J. Xu, J. A. Lewis, *Nature* **2004**, *428*, 386.
[195] L. E. Murr, E. V. Esquivel, S. A. Quinones, S. M. Gaytan, M. I. Lopez, E. Y. Martinez, F. Medina, D.H. Hernandez, E. Martinez, J. L. Martinez, S. W. Stafford, D. K. Brown, T. Hoppe, W. Meyers, U. Lindhe, R. B. Wicker, *Mater. Characterization* **2009**, *60*, 96.
[196] S. J. Murray, M. Marioni, S. M. Allen, R. C. O'Handley, T. A. Lograsso, *Appl. Phys. Lett.* **2000**, *77*, 886.
[197] V. A. Chernenko, M. Chmielus, P. Müllner, *Appl. Phys. Lett.* **2009**, *95*, 104103.
[198] T. Kakeshita, T. Fukuda, T. Takeuchi, *Mater. Sci. Eng. A* **2006**, *438–440*, 12.
[199] T. Kakeshita, T. Fukuda, Control of microstructure driven by magnetic field in ferromagnetic intermetallics, *Symposium II "Advanced Intermetallic-Based Alloys"*, Boston, MA, Materials Research Society, Warrendale, PA., 2006, p. II03-02.